WARSAW UNIVERSITY OF TECHNOLOGY

ENGINEERING AND TECHNOLOGY

MATERIALS ENGINEERING

Ph.D. Thesis

Mark Fedorov, M.Sc.

Phase stability and properties of Fe-Cr-Mn-Ni alloys from first-principles modeling

Supervisor

Prof. Krzysztof J. Kurzydłowski, dr hab. inż.

Additional supervisor

Dr. Jan S. Wróbel, dr inż.

WARSAW

Thanks to my supervisor Prof. Krzysztof J. Kurzydłowski for the support of all projects. Thanks to my assistant supervisor Dr. Jan S. Wróbel who taught me a lot and supported my creative approach to the tasks. Thanks to Dr. Duc Nguyen-Manh for frequent and fruitful discussions on virtually every part of my work. Thanks to everyone who encouraged me to pursue the degree. Thanks to my friends, who helped me emotionally, by hanging out online and sending me cat gifs.

This work was funded by the following projects:

HOMING project nr. Homing/2016-1/12 granted by Foundation for Polish Science, titled:

„Ab initio modeling of phase stability and properties of high entropy alloys”

"Modelowanie ab-initio stabilności fazowej i właściwości stopów o wysokiej entropii"

Materials Technologies project granted by Warsaw University of Technology under the program Excellence Initiative: Research University (ID-UB), titled:

„Ab initio modeling of phase stability of fcc and bcc high entropy alloys form the Fe-Cr-Mn-Ni system with experimental verification of the model”

"Modelowanie ab-initio stabilności fazowej stopów o wysokiej entropii RSC i RPC z układu Fe-Cr-Mn-Ni wraz z eksperymentalną weryfikacją modelu"

Abstract

The topic of high entropy alloys continues to gain momentum, as more findings indicate the important properties they possess in a wide variety of applications from biomaterials to aerospace engineering, at sizes ranging from nanoscale coatings to structural support, excelling in mechanical, catalytic, biocompatible, refractory, radiation-resistant and many other specific properties. The applicability of high entropy alloys is as vast as the phase space that should be searched to find them, and hence the new findings are coming at still increasing rate. The vast space, however, hides the gems well. Therefore, it is crucial to develop a good prediction algorithm, which would narrow down the search area or speed up the sampling of the search area.

The aim of this work is to theoretically investigate the phase stability of alloys from the Fe-Cr-Mn-Ni system, which are potential candidates for the nuclear fission and fusion applications due to their good mechanical and radiation-resistant properties. For this purpose, the prediction model for the Fe-Cr-Mn-Ni alloys with the face-centered cubic (fcc) and body-centered cubic (bcc) structures was developed in order to find potentially important compositions for the further investigation. The properties of alloys in the whole range of Fe-Cr-Mn-Ni system were investigated using the Density Functional Theory, Cluster Expansion model, Monte Carlo simulations and analyzed using known tools and the ones developed during this work. As the main result, the fcc-bcc phase diagram is constructed for Fe-Cr-Mn-Ni quaternary system and the region of disordered single fcc phase alloys is identified. The results of theoretical studies performed only based on first principles were validated by experiments performed at Faculty of Materials Science and Engineering.

Keywords: phase stability, high entropy alloy, *ab initio*, Monte Carlo simulations

Streszczenie

Stabilność fazowa i właściwości stopów Fe-Cr-Mn-Ni z modelowania z pierwszych zasad

Temat stopów o wysokiej entropii zyskuje na popularności, ponieważ coraz więcej odkryć wskazuje na pożądane właściwości jakie te stopy posiadają oraz możliwość ich szerokiego zastosowania, od biomateriałów po inżynierię lotniczą, w zależności od skali od powłok w nanoskali po materiały konstrukcyjne. Stopy o wysokiej entropii wyróżniają się właściwościami mechanicznymi, katalitycznymi, biokompatybilnymi, ogniotrwałymi, odpornością na promieniowanie i wielu innymi specyficznymi właściwościami. Możliwości ich zastosowania są tak rozległe, jak przestrzeń fazowa, którą należy przeszukać, aby je znaleźć, dlatego w coraz szybszym tempie rośnie liczba odkryć na ich temat. Ogromna przestrzeń jednak dobrze ukrywa klejnoty, dlatego tak ważne jest stworzenie dobrego algorytmu predykcyjnego, który zawęziłby obszar poszukiwań i przyspieszył wyznaczenie stopów o najlepszych, poszukiwanych właściwościach.

Celem niniejszej pracy było teoretyczne zbadanie stabilności fazowej stopów z układu Fe-Cr-Mn-Ni, które są potencjalnymi kandydatami do zastosowania w reaktorach jądrowych oraz syntezy termojądorowej, ze względu na ich dobre właściwości mechaniczne i podwyższoną odporność na promieniowanie. W tym celu opracowano model predykcyjny dla układów Fe-Cr-Mn-Ni o strukturze regularnej ściennie centrowanej (fcc) i przestrzennie centrowanej (bcc), który umożliwił wskazanie stężeń stopów o najlepszych właściwościach do dalszych badań. Właściwości stopów w całym zakresie układu Fe-Cr-Mn-Ni były badane przy użyciu obliczeń teorii funkcjonału gęstości, modelu Cluster Expansion, symulacji Monte Carlo oraz analizowane przy użyciu znanych i opracowanych w tej pracy narzędzi. Głównym wynikiem jest skonstruowanie diagramu fazowego fcc-bcc dla układu czteroskładnikowego Fe-Cr-Mn-Ni, na podstawie którego zidentyfikowano obszar występowania jednofazowych nieuporządkowanych stopów o wysokiej entropii o strukturze fcc. Wyniki badań teoretycznych prowadzonych wyłącznie na podstawie obliczeń z pierwszych zasad, były zwalidowane przy użyciu badań eksperymentalnych wykonywanych na Wydziale Inżynierii Materiałowej.

Słowa kluczowe: stabilność fazowa, stopy o wysokiej entropii, ab initio, symulacje Monte Carlo

Table of Contents

1 Introduction

1.1 Energy landscape trends

According to the Intergovernmental Panel on Climate Change's Sixth Assessment report [1], European countries are subject to climate-related issues, such as increased heat-related death of citizens and ecosystems, decreased crop yields, water scarcity and sea level rise. Although the risks are most noticeable for the southern Europe, Poland, having a coast and being 2nd European country by the area of farmlands [2], will be still susceptible to the projected climate change changes.

Per United Nations Environment Programme's Emission Gap Report 2022 [3], the main emission type contributing to the climate crisis remains to be fossil CO_2, coming from industries, relying on coal, oil and gas to thrive (see Fig. 1). And although the European Union holds the progressive policy on reducing CO_2 emissions and keeps improving, it remains one of the global major contributors.

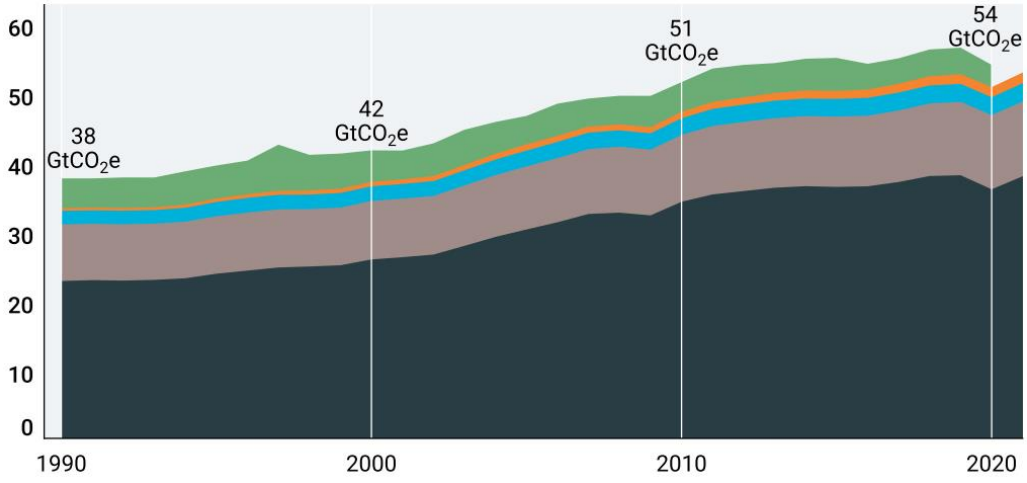

Fig. 1 Total greenhouse gas emission statistics. Source: Ref. [3].

The continuation of energy sector transformation is required to shift from relying on CO_2-producing fossil fuels, including transferring the burden to the offshore, and instead adapting to renewable and other energy sources, free from greenhouse gas emissions. As can be seen in Fig. 2, nuclear energy steadily allows to avoid CO_2 emissions. While renewable energy sources, such as wind and solar, are reactive to weather changes, and fusion reactors still being in the research, development and testing phase, nuclear reactors remain a stable and environmentally friendly energy source. Therefore, in order to achieve net zero emissions by 2050, extending the life of existing nuclear reactors, as well as building new ones is required, thus demanding innovation and investments in the field.

A positive side of nuclear-adjacent materials science is that its findings have the potential to be transferred to the area of fusion energy, as neutron irradiation is inherent to both families of technologies. As such, progress in nuclear materials inevitably transfers to fusion materials, potentially mitigating the climate crisis to a higher degree.

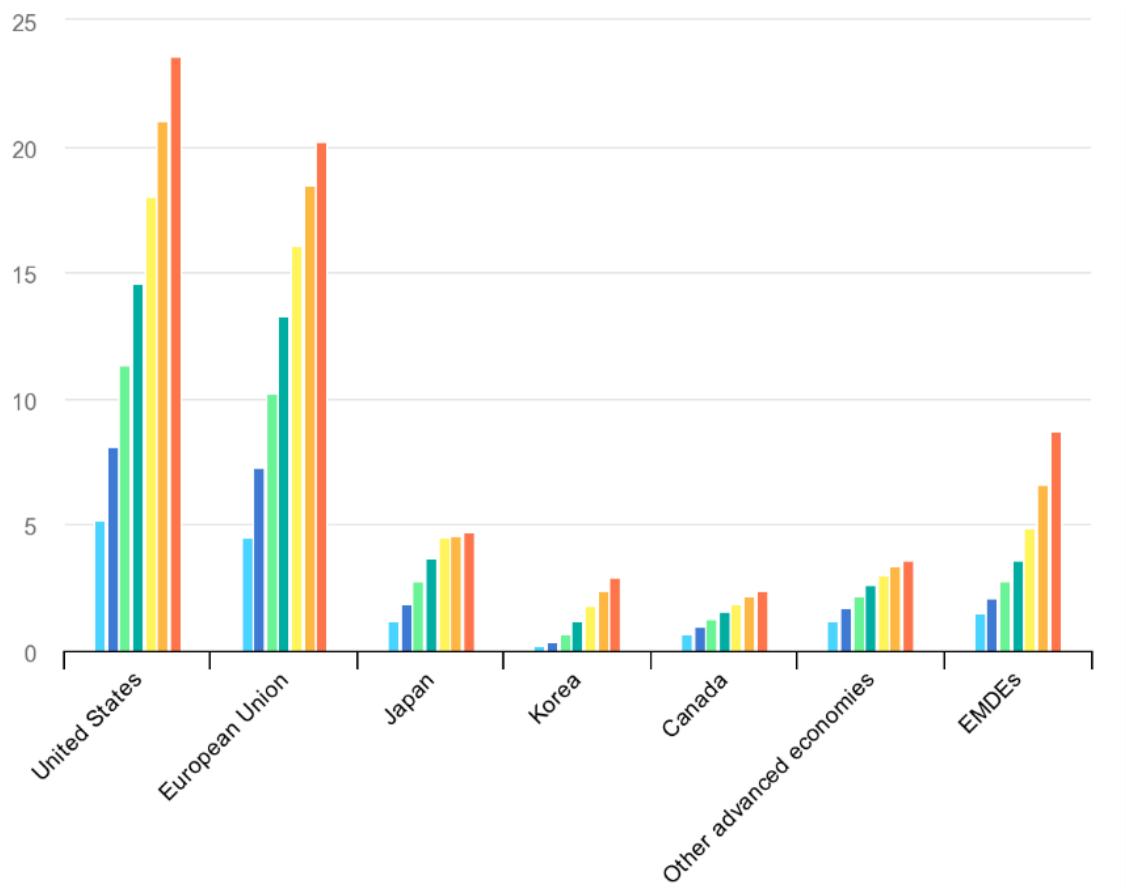

Fig. 2 Cumulative CO2 emissions avoided by nuclear power by country or region. Colors represent 5-year timespan since 1990 to 2020.

In view of the needs for materials for fusion power plants, the European DEMO design strategy and consequences for materials, published in 2017, can be chosen as the point of reference [4]. There, the best choice of plasma-facing materials is EUROFER and SS316 steel, both of which, despite having good mechanical properties, are subject to low-temperature embrittlement and radiation-induced volumetric swelling. Potential replacements for those materials are graphite, which is cheap and has good irradiation-resistant properties but is inapplicable as structural material, tungsten-based refractory alloys, which are radiation resistant and have good mechanical properties but are very expensive to produce, and high entropy alloys, which can optimally satisfy all 3 requirements.

1.2 Multi-principal-element alloys

The majority of traditional alloys can be described in the following way: one major component with alloying elements in small concentrations. Such an approach to understanding alloy materials has advanced humanity very far. However, knowing that all alloys have one or two major elements, combined with the knowledge that in near-equal concentrations, metals form intermetallic phases, which have limited applications, has left unexplored vast field of phase diagrams of multi-component metallic alloys, including the regions near the center of the phase diagrams.

A successful attempt of stranding away from such an approach to alloy design was officially published in 2004 independently by Yeh *et al.* [5] and Cantor *et al.* [6]. Cantor's alloy, as it is still known nowadays, is a CoCrFeMnNi alloy with each element having the same concentration, which is called an equiatomic alloy. In its as-cast state, it exists as a fully disordered single fcc phase solid solution and has great mechanical properties. The hypothesis behind why the alloy with multiple principal elements would not form an intermetallic phase and instead a disordered solid solution was the high configurational entropy. In thermodynamics, the stability of a phase is described via Gibbs free energy of mixing G_{mix}:

$$G_{mix} = H_{mix} - TS, \qquad 1.1$$

where H_{mix} is the mixing enthalpy of an alloy, T is the temperature, and S is the entropy. Negative Gibbs free energy means that the alloy is a stable form of existing for its components, whereas positive G_{mix} means that the alloys is not stable.

Entropy, being a measure of disorder, comes from different sources, such as disorder in the arrangement of elements – configurational entropy, disorder in magnetic moments – magnetic entropy, or disorder due to thermal oscillations and electronic excitations at finite temperatures – vibrational and electronic entropy, respectively. The configurational entropy of a perfectly-disordered solid solution is defined as follows:

$$S_{conf} = -k_B \sum_{i=1}^{N} c_i \, ln(c_i), \qquad 1.2$$

where c_i is the concentration of ith component in an N-component alloy, and k_B is the Boltzmann's constant (it is usually omitted, and the entropy is expressed in units of k_B). The maximum value of S_{conf} for any N-component alloy is achieved when the concentration of all elements is equal, $S_{conf} = -k_B \, ln\left(\frac{1}{N}\right) = k_B \, ln(N)$. The dependency is logarithmic, which means that the more elements are present in the alloy, the higher the configurational entropy will be (see Table 1 for S_{conf} of 2–6-element equiatomic alloys).

Table 1 Configurational entropies of N-component equiatomic alloys

N	S_{conf} [k_B]
2	0.693
3	1.099
4	1.386
5	1.609
6	1.792

Since configurational entropy contributes to the lowering of Gibbs free energy of mixing in Eq. 1.1, the alloys with more elements with equal composition will have higher configurational entropy that will stabilize the random solid solution. Due to this reasoning, such alloys are currently classified in the literature as High Entropy Alloys (HEAs).

1.2.1 State of the art

High entropy alloys research increases every year, as indicated by a number of articles (see Fig. 3).

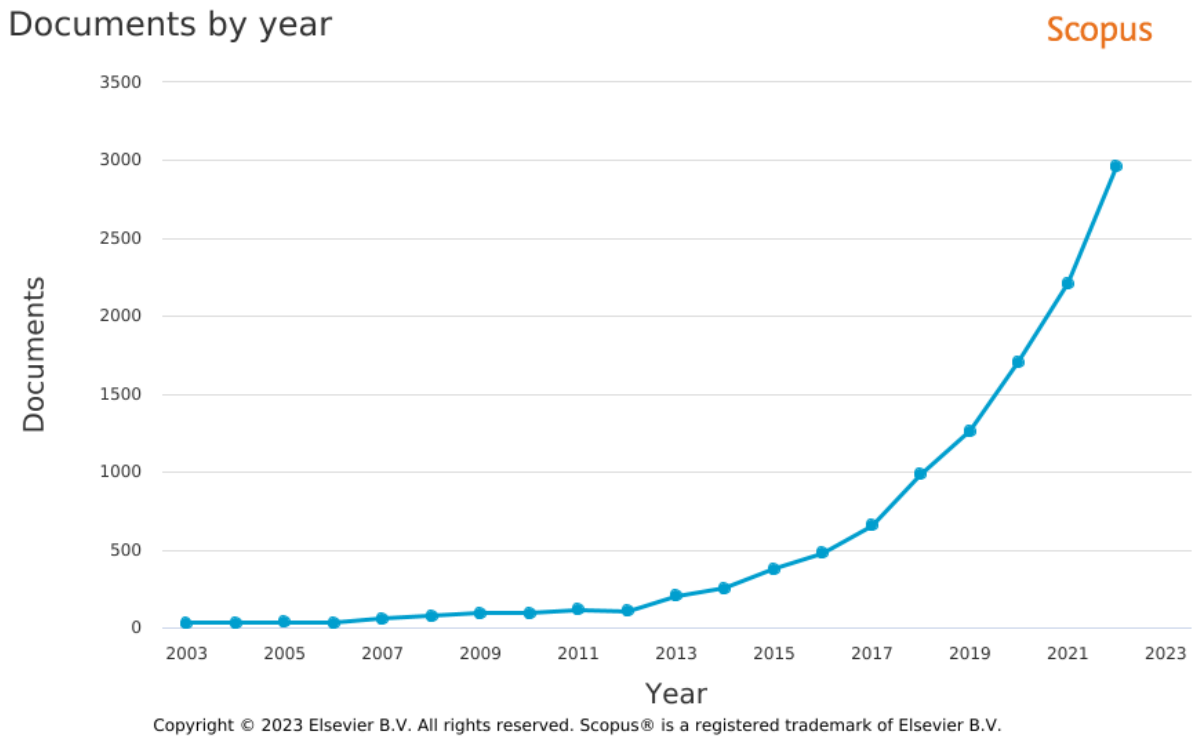

Fig. 3 Number of documents containing the term "high entropy alloys" in the title, abstract or keywords in the last 20 years.

Various methods for obtaining HEAs are being developed, such as spark plasma sintering [7].

Original effects proposed to exist in HEAs [8] have been investigated thoroughly and are often reported to be elusive in various HEAs [9]. Nevertheless, investigation of HEAs has resulted in new alloys with improved properties such as high corrosion resistance [10], yield strength [11–13], and compressive strength [14]. Of interest in this work are the high entropy alloys which have the potential application under irradiation.

$Cr_{15}Ta_{36}V_{11}W_{38}$ alloy has shown no signs of the formation of irradiation-induced dislocation loops as well as no effects of irradiation hardening after 8 dpa [15].

$Cr_{18}Fe_{27}Mn_{27}Ni_{28}$ under irradiation of 0.03–10 dpa had high-density small dislocation loops, but no voids, which resulted in nonexistent irradiation-induced swelling, and sluggish diffusion resulted in limited migration of solutes to grain boundaries [16]. Later theoretical investigation of said alloy [17] indicated a large spread of the normal distribution of vacancy formation energies with no significant dependency on atomic sort of vacancy.

The effect of compositional complexity on irradiation-induced swelling has been systematically investigated for Ni and equiatomic NiCo, NiFe, NiCoFe, NiCoCr, NiCoFeCr and NiCoFeCrMn alloys irradiated at 500 °C with peak damage between 4 and 60 dpa [18,19]. Void size reduces with the number of elements (see Fig. 4), with irradiation tolerance of NiCoFeCrMn being 40 times larger compared to pure Ni. Authors of [19] suggested the mechanism behind such behavior: easier recombination of defects due to less limited short-range movement of defects.

Summarizing the above experiments, HEAs can possess outstanding radiation properties, and thus they are interesting candidates as structural materials for nuclear applications. Especially, Fe-Cr-Mn-Ni HEAs can potentially replace the austenitic steels as 304 and 316 steels, which are used, for example, as structural materials for fast breeder and light water and fission reactors [20,21]. However, as presented in experimental studies in Refs. [16,22–34], the phase stability of Fe-Cr-Mn-Ni alloys is complex and it depends on the composition of an alloy. For example, there was observed a decomposition into the fcc and bcc phases for the equiatomic FeCrMnNi alloy [24,25,29,30] and the $Cr_xFeMnNi$ alloys, where $x = 0.8, 1.0, 1.2, 1.5$ [25]. The other effect was reported in Ref. [27] for the irradiated $Fe_{29}Cr_{18}Mn_{23}Ni_{30}$ alloy, namely the formation of MnNi precipitates, which might degrade the mechanical properties of an alloy. Since the best mechanical and radiation properties are observed for fcc alloys without precipitations of intermetallic phases and coexistence with bcc alloy, it is crucial to understand the effect of alloy composition and temperature on the phase

stability of Fe-Cr-Mn-Ni alloys. Due to the incredibly vast amount of potential alloy compositions, the most viable path of investigating multi-principal element alloys is modeling [35].

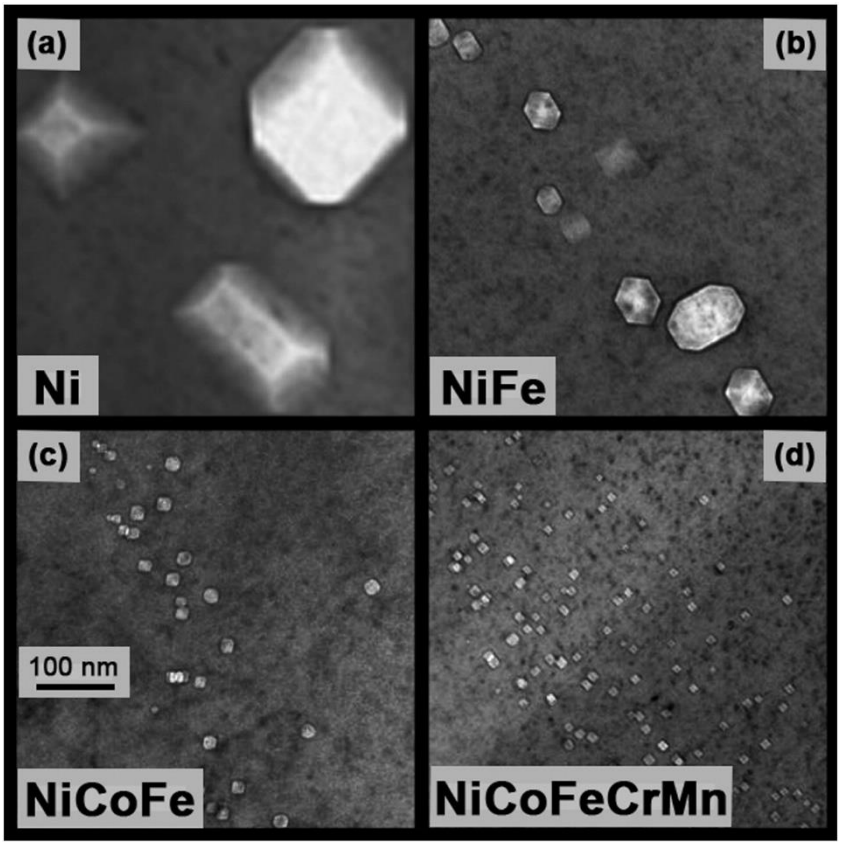

Fig. 4 TEM images of the maximum swelling region of (a) Ni, (b) NiFe, (c) NiCoFe, and (d) NiCoFeCrMn irradiated to a fluence of 5×10^{16} cm^{-2} at 500 °C. Source: Ref. [18].

2 Objectives, hypothesis, and scope of the work

As it was described in the previous section, the Fe-Cr-Mn-Ni multi-principal element alloys are a novel group of materials that are potential candidates as structural materials for nuclear applications. However, the phase stability and properties of alloys in the Fe-Cr-Mn-Ni system are still not known very well. Therefore, there is a need for their theoretical description.

Hypothesis in this work is following: there exist unidentified multi-principal element alloys in the Fe-Cr-Mn-Ni system possessing stable disordered single fcc phase that can be found with a purely theoretical approach.

Aim of this work is thus to describe the phase stability and chosen properties of Fe-Cr-Mn-Ni alloys in the whole composition range and identify promising alloy compositions from first principles.

In order to achieve the aim of the work, the following tasks need to be accomplished:

- Creation of extensive database for the most stable phases predicted in the investigated system, namely face-centered cubic (fcc) and base-centered cubic (bcc)
- Calculation of formation energies from first principles for all structures in the database
- The development of cluster expansion (CE) models for fcc and bcc Fe-Cr-Mn-Ni alloys
- Simulation of atomic structure and Gibss free energies of formation for fcc and bcc of alloys on nanoscale at finite temperatures using the developed CE models
- Multi-dimensional analysis of Gibbs free energies of formation and the estimation of the fraction of fcc phases in Fe-Cr-Mn-Ni alloys as a function of alloy composition and temperature.

3 Methodology

The methodology applied in this work includes a set of methods, which start from quantum-mechanics-based calculations of phase stability at absolute zero, and end with finite-temperature Monte Carlo simulations.

3.1 Density Functional Theory

On the energy scales outside of the specific laboratories, the physical properties of materials are governed by the rules of quantum mechanics. Quantum mechanical interactions define the structure and properties of materials. Although in the real world the temperatures are finite, the temperature-related interactions only modify the basic state of the system – its ground state.

The ground state of a quantum-mechanical system can be described by the time-independent Schrödinger equation:

$$\widehat{H}\psi_{\mathrm{N}} = E\psi_{\mathrm{N}} \tag{3.1}$$

where ψ_N is the many-body wavefunction describing the system, $\widehat{H}$ is the operator of total energy, called Hamiltonian, and E is the eigenvalue of the total energy of the system.

Many-body system in the context of materials science refers to material consisting of ions and electrons, hence, total energy of such system is defined as follows:

$$\widehat{H} = -\frac{\hbar^2}{2M_i}\sum_i \nabla_i^2 - \frac{\hbar^2}{2m}\sum_j \nabla_j^2 + \frac{1}{2}\sum_{i,k}^{i\neq k}\frac{Z_i Z_k e^2}{|r_i - r_k|} + \frac{1}{2}\sum_{j,l}^{j\neq l}\frac{e^2}{|r_j - r_l|} - \sum_{i,j}\frac{Z_i e^2}{|r_i - r_j|}, \tag{3.2}$$

where $\hbar$ is the Planck's constant normalized by 2π, M and m are masses of ions and electrons, respectively, Z is the charge of ion, e is the charge of electron, and r is the position of each element in space. The first and second terms describe the kinetic energy of ions and electrons, respectively. The last three terms describe the potential energy between ions, electrons and the interaction between ions and electrons, respectively, all in form of Coulomb interactions.

Such a form of Hamiltonian, when applied to Eq. (3.1), provides the exact description of the system. However, the complexity of such an equation is $\mathcal{O}(N^2)$, where $N = N_{ion} + N_{elec}$ is the number of all particles in the system, including ions and electrons. The time of solving such an equation analytically quickly increases with the size of the system. For practical

application to the investigation of real materials, the analytical solution is unreasonable. As such, approximations should be introduced to achieve practicality.

The first such approximation was introduced by **Born and Oppenheimer** in 1927 [36]. The Born-Oppenheimer approximation states that since the typical ratio of electron mass to ion mass is on the order of 10^4, the relaxation times for ions are much larger than the relaxation times for electrons, and as such, the wavefunction ψ_N of a many-body system can be separated into two subsystems – of ions and electrons, and when treating the electrons subsystem, the ions can be safely assumed to be static. Therefore, only the second, fourth and fifth members of Eq. (3.2) are considered in the electrons system Hamiltonian:

$$\hat{H} = -\frac{\hbar^2}{2m}\sum_j \nabla_j^2 + \frac{1}{2}\sum_{j,l}^{j\neq l}\frac{e^2}{|r_j - r_l|} - \sum_{i,j}\frac{Z_i e^2}{|r_i - r_j|}, \qquad 3.3$$

which represents the kinetic, internal potential energy and external potential energy (coming from ionic subsystem):

$$\hat{H} = \hat{T} + \hat{V}_{int} + \hat{V}_{ext}. \qquad 3.4$$

In 1964 in the seminal paper by **Hohenberg and Kohn** [37], which is considered the beginning of Density Functional Theory (DFT), important insights were introduced regarding treating Hamiltonian (3.3) via the electron density in the form of two following theorems.

Theorem 1 states that the external potential $v(r)$ that defines potential energy V_{ext} is a unique functional of the ground-state electron density $n(r)$.

It should be noted that functional is a concept similar to function, with an additional layer of dependency. A function is a rule relating two sets of values, mapping each number in the input set to a number in an output set. A functionals output set also consists of numbers, however, the input set consists of functions. In other words, a functional is a function of a function. In order to distinguish functions and functionals in mathematical notation, function arguments are written in parentheses, $f(x)$, while functional arguments are written in square brackets, $F[f(x)]$.

Since the eigenvalue of Hamiltonian – the energy of the ground state – depends on the potential energy, it is also a functional of electronic density:

$$\begin{aligned} E[n(r)] &= \langle\psi|\hat{H}|\psi\rangle = \langle\psi|\hat{T} + \hat{V}_{int} + \hat{V}_{ext}|\psi\rangle \\ &= T[n(r)] + V_{int}[n(r)] + V_{ext}[n(r)]. \end{aligned} \qquad 3.5$$

Theorem 2 states that since ground-state energy $E[n(r)]$ is the minimal energy of the system, the ground-state electronic density $n(r)$ should minimize $E[n(r)]$ according to the variational principle.

Additionally, **Hohenberg and Kohn** [37] have noted that $T[n(r)] + V_{int}[n(r)]$ only describe interaction of electrons, and these terms are agnostic to the ions they are attached to. As such, there should exist a universal functional $F[n(r)] = T[n(r)] + V_{int}[n(r)]$, valid for any system of ions and electrons. Lastly, they separated the well-known part of universal functional, the Coulomb interactions term, and leave the other effects in second universal functional $G[n(r)]$:

$$F[n(r)] = \frac{1}{2}\int \frac{n(r)n(r')}{|r-r'|}drdr' + G[n(r)] \qquad 3.6$$

where the first term describes Coulomb interaction via electron densities at points r and r'.

As such, a direction of finding the ground state was defined. However, the complexity of the equation remained the same – $\mathcal{O}(N_{elec}^2)$ and impractical, and the form of the universal functional was not yet introduced.

In the following work in 1965 by **Kohn and Sham** [38], they proposed that $G[n(r)]$ can be approximated in the following form:

$$G[n(r)] = T_s[n(r)] + E_{xc}[n(r)] \qquad 3.7$$

where $T_s[n(r)]$ is the kinetic energy of a system of non-interacting electrons with electron density $n(r)$, and $E_{xc}[n(r)]$ is the exchange and correlation energy of an interacting system of electrons with density $n(r)$ – in a sense, a correction term. **Kohn and Sham** then proposed that for a system with sufficiently slowly varying electron density, the form of exchange-correlation can be expressed via exchange-correlation energy per electron of a homogeneous electron gas, $\epsilon_{xc}\big(n(r)\big)$, as following:

$$E_{xc}[n(r)] = \int n(r)\epsilon_{xc}\big(n(r)\big)dr. \qquad 3.8$$

Electron density of a system of N non-interacting electrons can be found by:

$$n(r) = \sum_{i=1}^{N} |\psi_i(r)|^2, \qquad 3.9$$

where ψ_i are one-electron wavefunctions. The, in turn, can be found by solving the one-electron Schrodinger equations:

$$\left\{-\frac{1}{2}\nabla^2 + \left[v(r) + \int \frac{n(r')}{|r-r'|}dr + \frac{d\big(n\epsilon_{xc}(n)\big)}{dn}\right]\right\}\psi_i(r) = \epsilon_i\psi_i(r). \qquad 3.10$$

Equations 3.9 and 3.10 are dependent on each other, so they should be solved self-consistently. One can start with reasonably assumed $n(r)$, solve Eq. 3.10, and find new $n(r)$

from Eq. 3.9. The procedure should be repeated until the new $n(r)$ is almost indistinguishable from $n(r)$ obtained at the previous step, which will be the ground-state electron density.

With the approximated form of universal functional, the ground state can be found, and the ground-state energy will be calculated and used for multiple purposes. Additionally, since the electron system is not represented by one N-body wavefunction, but with N one-body wavefunctions, the complexity of solution drops to $\mathcal{O}(N_{elec})$.

It should be noted here, that it is practically impossible to calculate the properties of a real physical object using the quantum mechanical approach that includes the treatment of electrons. However, crystal structures are periodical, and therefore their properties can be represented by a unit cell, which, if translated, reproduces the real material. Since calculations of energy involve wavefunctions, which are usually better dealt with in momentum space (or reciprocal space). And due to periodicity, they can be similarly represented by periodic wavefunction in a unit cell, called the first Brillouin zone. In 1976, **Monkhorst and Pack** [39] introduced a way to choose special points in the Brillouin zone in order to efficiently integrate periodic wavefunctions.

With time passing, there has been developed a zoo of approximations, one building on another. The first most important is the pseudopotential approximation from 1990 by **Vanderbilt** [40], which has shown that treating only valence electrons in the previously described manner while treating electrons on inner shells as a parameter reproduces material properties with the same precision as all-electron calculations, but significantly reduces the time for calculations. The second most important method was proposed in 1994 by **Blöchl** [41], which proposed to represent electron wavefunction in a plane-wave projector basis.

The assumption of homogeneous electron density [38], called local density approximation, works indeed well for systems with homogeneous electron density, which includes bulk metals. However, for non-uniform materials, such an assumption is incorrect. One of the ways the non-uniformity can be taken into account is by including the dependency on the gradient of electron density into exchange-correlation energy ϵ_{xc}. Such dependency was implemented in different functionals, which are grouped into generalized gradient approximations family. One of such functionals, suitable for non-uniform solid materials, was introduced in 1997 by **Perdew, Burke and Ernzerhof** [42], referred to as PBE, and is widely used nowadays since it parametrizes the exchange-correlation functional, making calculations fast.

There are many practical implementations of the discussed methods, including open source, closed-source, commercial and free programs. The “industry standard” for alloys is a

program developed by **Georg Kresse** and colleagues [43–45], called Vienna Ab-initio Simulation Package (VASP), which is applied for DFT calculations in this work.

3.2 Phase stability at absolute zero

At absolute zero, the $-TS$ term from Gibbs free energy (Eq. 1.1) is equal to zero, and the stability of the substance or material can be defined solely via the **enthalpy of mixing**:

$$H_{mix} = E_{alloy} - \sum_i x_i E_i, \tag{3.11}$$

where E_{alloy} is the total energy of the alloy, x_i is the concentration of ith component of the alloy, and E_i is the total energy of the pure ith component.

Negative mixing enthalpy of an alloy means that such form of existence is preferable for the considered components, whereas an alloy with positive mixing enthalpy is less preferable compared to existing in the form of segregated pure components. In the context of solid phases, the definition of H_{mix} is more narrowly applied for the cases where alloy and its components have the same crystal lattice. In practice, alloys are often composed from elements that in their pure state exist in form of different crystal lattices. Therefore, a thermodynamic potential that better describes the stability of the alloy is introduced, which is called the **formation enthalpy** and is defined as:

$$H_{form} = E_{alloy}^{alloy\ lattice} - \sum_i x_i E_i^{stable\ lattice\ of\ i}. \tag{3.12}$$

Formation enthalpy is a useful parameter in the framework of theoretical materials design since it allows one to estimate the phase stability of any considered alloy by constructing a **convex hull diagram** for virtually any phase, as it is presented is Fig. 5.

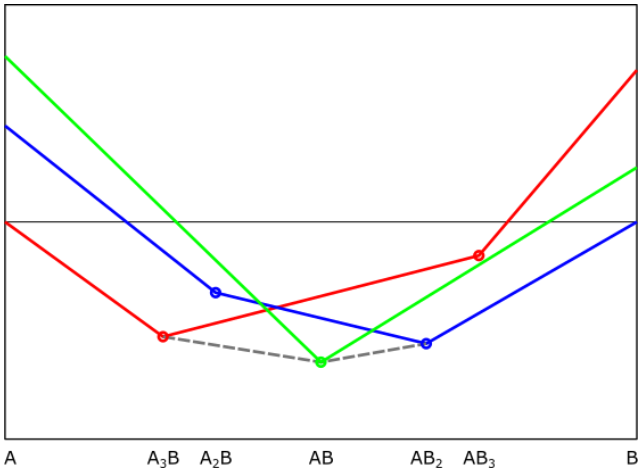

Fig. 5 Convex hull diagram for 3 crystal lattices defined by solid lines. Dashed line fills the gap between the convex hulls of each crystal lattice to form the global convex hull for the alloy.

Having such a convex hull diagram, one can predict stable, unstable, and meta-stable phases for the considered alloy. Since H_{form} can be calculated for virtually any phase and composition, one should limit themselves in both, at least at the starting point of the model construction, in order to obtain the results in a reasonable time.

Although the proposed methodology does not include empirical approaches, it would be unreasonable to ignore the available experimental data for the system one is investigating if it exists. As such, available experimental data on observed phases in the system can be a good choice for phases to be modelled. The choice of composition can also be decided on off compositions of experimentally observed phases.

For multi-component systems, the initial set of structures and compositions based on known experimental phases is usually much sparser compared to two-component systems. It can be expanded by constructing additional structures based on low-symmetry two-component structures with more than 2 Wyckoff positions – positions that are unique under all symmetry operations in the considered structure – which can be populated by atoms of the multi-component system of interest.

The convex hull diagram, described in this subsection, is useful, but is limited to absolute zero, which is not particularly practical for predicting the phase stability of materials applied in real structures at real conditions. In order to investigate finite-temperature phase stability, different methods exist, which include finite-temperature DFT, molecular dynamics and Monte Carlo simulations. While finite-temperature DFT methods continue to keep the quantum-mechanical level precision, they require additional approximations and additional calculations, which are time-consuming and impractical for investigating the properties of multi-component alloys in the whole composition range. Molecular dynamics simulations require potentials that differ depending on the elements present in the system and not rarely have to be constructed for one's system of interest by performing additional DFT calculations. Lastly, exchange Monte Carlo simulations require set of rules, for example interactions between the elements, for calculating the energy of the system. Such interactions may be constructed based purely on DFT calculations that were performed for the construction of convex hull diagram by means of Cluster Expansion.

3.3 Cluster Expansion model

Cluster expansion (CE) formalism is based on the description of configurational cluster functions in terms of an orthogonal basis of discrete spin variables in multidimensional space, introduced by **Sanchez** *et al.* in Ref. [46]. The approach is the extension of the well-

known Ising Hamiltonian, used initially for the investigation of ferromagnetic ordering in crystal lattices, which assumes the fixed lattice and defines the spin variable for each site. Cluster expansion also operates with the fixed lattice and spin-like occupation variables σ_i for each site i on the lattice. Each configuration of atoms in the lattice can be represented by a vector of occupational variables $\boldsymbol{\sigma}$, and the energy of the configuration can be described with the Hamiltonian in terms of occupational variables:

$$H(\boldsymbol{\sigma}) = \sum_{\alpha} m_\alpha J_\alpha \langle \Gamma_{\alpha'}(\boldsymbol{\sigma}) \rangle \qquad 3.13$$

where α is a subset of sites i – a cluster. The summation is performed over all clusters α that are distinct by symmetry. The averaging is performed over all clusters α' that have identical symmetry to α, the number of which is represented by m_α, called multiplicity. The energy contribution of each cluster to the total energy is contained in the coefficient J_α, which is called effective cluster interaction (ECI). Lastly, the $\Gamma_{\alpha'}(\boldsymbol{\sigma})$ is the cluster function.

For binary alloy, the occupational variables σ_i can assume the values of 1 and -1, and the cluster functions are then simply the product of the occupational variables, $\Gamma_{\alpha'}(\boldsymbol{\sigma}) = \Pi_{i \in \alpha'}(\sigma_i)$. For multi-component systems with K components, the generalized cluster functions can be defined via the point functions of occupation variables, $\gamma_{\alpha_i, K_i}(\sigma_i)$, as follows:

$$\Gamma_{\alpha'}(\boldsymbol{\sigma}) = \prod_i \gamma_{\alpha_i, K_i}(\sigma_i) \qquad 3.14$$

where the point functions $\gamma_{\alpha_i, K_i}(\sigma_i)$ are defined, according to Ref. [47], as follows:

$$\gamma_{\alpha_i, K_i}(\sigma_i) = \begin{cases} 1 & \text{if } \alpha_i = 0 \\ -cos\left(2\pi \left\lceil \frac{\alpha_i}{2} \right\rceil \frac{\sigma_i}{K}\right) & \text{if } \alpha_i > 0 \text{ and odd} \\ -sin\left(2\pi \left\lceil \frac{\alpha_i}{2} \right\rceil \frac{\sigma_i}{K}\right) & \text{if } \alpha_i > 0 \text{ and even} \end{cases} \qquad 3.15$$

where α_i and σ_i both range from 0 to $K - 1$, and the $\lceil \cdots \rceil$ brackets stand for the ceiling function – an operation of rounding up a value inside the brackets to the closest integer.

In theory, if all clusters α are considered in the cluster expansion and given the correctly chosen values of effective cluster interactions J_α, the total energy of any configuration $\boldsymbol{\sigma}$ obtained via Eq. 3.13 should correspond to the value of total energy, obtained through the quantum-mechanical calculations described in Section 3.1. In practice, the cluster expansion converges rapidly, meaning that only relatively small clusters can be considered in order to reproduce the total energy. Knowing this fact, it was proposed by **Connolly and Williams** [48] that atomic interactions can be found by fitting them to a set of structures, calculated using more precise methods, such as DFT. This method is called a Connolly-Williams method or structure

inversion method. It is then up to the researcher to decide which structures to fit and where to truncate the series of cluster expansion. Such a decision is quite cumbersome and time-consuming, which motivated **van de Walle, Asta and Ceder** to create an algorithm that finds optimal cluster expansion based on cross-validation and variance reduction. This algorithm is implemented as the Multicomponent MIT Ab-initio Phase Stability code (`mmaps`) [49] from the Alloy Theoretic Automated Toolkit (ATAT), developed by [50]. This software is used in the current work for the fitting of the cluster expansion model.

3.4 Monte Carlo simulations

With ECIs known, the Hamiltonian from Eq. 3.13 may be used to calculate the energy of a significantly larger cells compared to the ones used for fitting the said Hamiltonian. In practice, since a statistical approach should be applied for simulations, the reasonable size of configurations is 1–2 orders of magnitude larger than the limits of DFT calculations.

Canonical exchange Monte Carlo simulations are performed on lattice for the supercell, where the number of particles stays the same. At each temperature T, a number of exchanges of neighboring atoms in the lattice are performed. If an exchange leads to a configuration with a decreased total energy of the system, $\Delta E < 0$, it is accepted. If instead it leads to an increased total energy of the system, $\Delta E > 0$, it is accepted with probability $exp\left(-\frac{\Delta E}{k_B T}\right)$. The energy is then averaged over all exchanges and the new atomic configuration is passed to the simulations with a different temperature. In theory, one can start either from low or high temperature and increase or decrease it, respectively, in the consequential simulations. However, since atomic configuration at low temperature is not known for the vast majority of the compositions which are of interest of this work, as well as in other exploratory theoretical investigations, usually the simulations start at high temperature, where the atomic configuration can be reasonably approximated with a fully disordered structure, and the temperature is decreased in what is called a simulated annealing procedure.

An easy tool for performing Monte Carlo simulations have been also developed by **van de Walle, Asta and Ceder** in the form of Multicomponent Easy Monte Carlo Code (`memc2`) [51] packed in the ATAT [50], which is used for Monte Carlo simulations in this work.

3.5 Phase stability at finite temperatures

At finite temperatures, the phase stability is not defined solely through H_{mix}, but is also influenced by $-TS$ term in Eq. 1.1. As it has been noted in Section 1.2, entropy comes

from various sources, including configurational, vibrational, magnetic, and electronic contributions:

$$S(T) = S_{conf}(T) + S_{vib}(T) + S_{mag}(T) + S_{el}(T) \qquad 3.16$$

Each entropic contribution, apart from configurational, requires additional time-consuming first-principle calculations. In order to make the computational times reasonable, it is necessary to estimate the importance of each term from the point of view of the main goal of this work – the investigation of the relative phase stability of alloys on different lattices. Since Configurational entropy $S_{conf}(T)$ depends on the configuration of atoms and varies significantly with composition, temperature, and crystallographic lattice, hence it may give significant differences for two compositions below the high-temperature limit. Vibrational entropy is dependent on the type of atoms and is expected to be similar for different phases at the same temperature and composition. The difference in magnetic entropy is also expected not to be significant above Curie temperatures of the materials. Electronic entropy difference is also not significant for different phases at the same temperature and composition. A similar estimation has been reported in [9,52–56]. Since the main interest of this work also lies in the middle of the quaternary phase diagram, where configurational entropy is high, only $S_{conf}(T)$ is decided to be reasonable to take into account.

While the **Bragg-Williams** approximation [57] for entropy (Eq. 1.2) represents the fully disordered solid solution and gives the maximum estimate for the entropy for given composition, at lower temperatures, short-range order should be reflected in the lowering of configurational entropy. Such contribution is present in the **Bethe-Guggenheim** quasi-chemical approximation [58,59]:

$$S_{conf}(\boldsymbol{\sigma}, T) = S_{ideal}(\boldsymbol{\sigma}) - \sum_n \frac{z_n}{2} I_n(\boldsymbol{\sigma}, T), \qquad 3.17$$

where the first term is calculated using Eq. 1.2 for the given configuration, z_n is the coordination number for shell n in the given crystallographic lattice, and $I_n(\boldsymbol{\sigma}, T)$ contains the information about pair bonds at nth shell:

$$I_n(\boldsymbol{\sigma}, T) = \sum_{ij} y_{2,n}^{ij}(\boldsymbol{\sigma}, T) \ln \frac{y_{2,n}^{ij}(\boldsymbol{\sigma}, T)}{c_i c_j} \qquad 3.18$$

where the summation is performed over all pairs of components in the system, c_i and c_j are the concentrations of ith and jth components, respectively, and $y_{2,n}^{ij}(\boldsymbol{\sigma}, T)$ are the pair (2-body) probability functions describing the probability of finding atomic species i in the nth shell of species j.

In order to arrive at the simpler form of Eq. 3.17, $I_n(\boldsymbol{\sigma}, T)$ can be rewritten in the following manner. First, terms under logarithm coming from concentrations and pair probability functions should be separated:

$$I_n(\vec{\sigma}, T) = \sum_{ij} y_{2,n}^{ij} \left(\ln y_{2,n}^{ij} - \left(\ln c_i + \ln c_j \right) \right)$$

$$= \sum_{ij} y_{2,n}^{ij} \ln y_{2,n}^{ij} - \left(\sum_{ij} y_{2,n}^{ij} \ln c_i + \sum_{ij} y_{2,n}^{ij} \ln c_j \right) \qquad 3.19$$

$$= \sum_{ij} y_{2,n}^{ij} \ln y_{2,n}^{ij} - \left(\sum_{i} \ln c_i \sum_{j} y_{2,n}^{ij} + \sum_{j} \ln c_j \sum_{i} y_{2,n}^{ij} \right) = *$$

Since pair probabilities satisfy sum rule, $\sum_j y_{2,n}^{ij} = c_i$, we can rewrite it further as:

$$* = \sum_{ij} y_{2,n}^{ij} \ln y_{2,n}^{ij} - \left(\sum_{i} \ln(c_i)\, c_i + \sum_{j} \ln\left(c_j\right) c_j \right) = ** \qquad 3.20$$

and since i and j iterate over the same components:

$$** = \sum_{ij} y_{2,n}^{ij} \ln y_{2,n}^{ij} - 2 \sum_{i} c_i \ln c_i. \qquad 3.21$$

It is clear that the last term is equal to $2S_{ideal}(\vec{\sigma})$, so substituting Eq. 3.21 and Eq. 1.2 into Eq. 3.17 yields the following:

$$S_{conf}(\boldsymbol{\sigma}, T) = -\sum_{i} c_i \ln c_i - \sum_{n} \frac{z_n}{2} \left(\sum_{ij} y_{2,n}^{ij} \ln y_{2,n}^{ij} - 2 \sum_{i} c_i \ln c_i \right) =$$

$$= \left(\sum_{n} z_n - 1 \right) \sum_{i} c_i \ln c_i - \sum_{n} \frac{z_n}{2} \sum_{ij} y_{2,n}^{ij} \ln y_{2,n}^{ij}. \qquad 3.22$$

In order to find pair probability functions, one can iterate over every atom in the simulation cell and count them automatically. However, a matrix formulation of point probabilities, described in Ref. [60], allows for a simpler calculation using quantities naturally occurring during the construction of cluster expansion.

First, it is better to define cluster functions $\Gamma_{\alpha'}(\boldsymbol{\sigma})$ in more detailed notation, specifying the number of lattice sites in the cluster, ω, the maximum distance between two sites in the cluster, n, as $\Gamma_{\omega',n'}(\boldsymbol{\sigma})$. The generalized equation for cluster functions, then, may be expressed in terms of probability functions as follows:

$$\langle \Gamma_{\omega',n'}(\boldsymbol{\sigma}) \rangle = \sum_{ij\cdots} \left({}^{\otimes}\prod_{\omega} (\bar{\bar{\tau}}_K)\, y_{\omega,n}^{ij\cdots} \right) \tag{3.23}$$

where ${}^{\otimes}\prod_{\omega}(\bar{\bar{\tau}}_K)$ is a consequent Kronecker product, also called matrix direct product, of a matrix $\bar{\bar{\tau}}_K$, which is constructed from point functions $\gamma_{\alpha_i,K_i}(\sigma_i)$ in a following manner:

$$\bar{\bar{\tau}}_K = \begin{bmatrix} \gamma_{0,K}(0) & \cdots & \gamma_{0,K}(K-1) \\ \vdots & \ddots & \vdots \\ \gamma_{K-1,K}(0) & \cdots & \gamma_{K-1,K}(K-1) \end{bmatrix}. \tag{3.24}$$

Since cluster functions $\Gamma_{\omega,n}(\sigma_{\alpha'})$ are calculated during cluster expansion, inversion of Eq. 3.23 will help to find probability functions $y_{\omega,n}^{ij\cdots}$ with the help of the fact that inverse of a matrix direct product is equivalent to the matrix direct product of inverse matrices. The elements of the inverse matrices $\bar{\bar{\tau}}_K^{-1}$ are constructed from the following elements:

$$\tilde{\gamma}_{\alpha_i,K_i}(\sigma_i) = \begin{cases} 1 & \text{if } \alpha_i = 0 \\ -2sin\left(2\pi \left\lceil \frac{\alpha_i}{2} \right\rceil \frac{\sigma_i}{K}\right) & \text{if } \alpha_i > 0 \text{ and even} \\ -2cos\left(2\pi \left\lceil \frac{\alpha_i}{2} \right\rceil \frac{\sigma_i}{K}\right) & \text{if } \mathrm{K}-1 > \alpha_i > 0 \text{ and odd} \\ -cos\left(2\pi \left\lceil \frac{\alpha_i}{2} \right\rceil \frac{\sigma_i}{K}\right) & \text{if } \alpha_i = \mathrm{K}-1 \text{ and odd.} \end{cases} \tag{3.25}$$

As such, probability functions can be found using cluster functions as:

$$y_{\omega,n}^{ij\cdots} = \sum_{ij\cdots} \left({}^{\otimes}\prod_{\omega} (\bar{\bar{\tau}}_K^{-1}) \langle \Gamma_{\omega',n'}(\boldsymbol{\sigma}) \rangle \right) \tag{3.26}$$

and used for the calculation of configurational entropy.

Even more generalized form of entropy contribution shown in Eq. 3.22, which would include 3- and 4-body probability functions, have been proposed in Ref. [60]. However, it has been demonstrated in the same work that for $y_{\omega,n}^{ij\cdots}$ with $\omega > 2$, configurational entropy quickly drops into negative values below certain temperature, related to order-disorder transition.

3.6 Gibbs free energy analysis for multi-component systems

The accepted method for studying multi-component systems is CALPHAD. This method is based on Gibbs free energy calculations determined from the Gibbs free energy of each component as well as multi-component interaction terms. Gibbs free energy is as such represented as a series of Legendre polynomials, which are fitted to input data. This continues the line of concentration-independent methodology, but the drawback is such that fitting cannot always represent the input data. This happens when the input data has a more rigid shape instead

of a polynomial. This, in turn, is especially noticeable when the ordered phases are present in the system.

The alternative to CALPHAD method is the extended version of the common tangent construction. This method, although not fully physical, lacks the drawback of being dependent on fitted equations and instead operates on exact input data.

When applied to finding the phase composition in binary alloys, this method reproduces the well-known common tangent construction with the consequent common tangent construction (see schematic in Fig. 6).

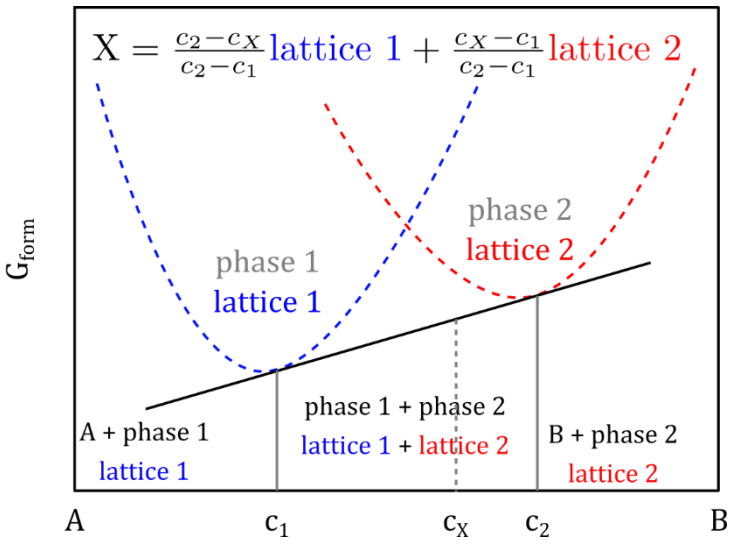

Fig. 6 Common tangent construction for binary alloy.

For multi-component systems, one can separate the composition space into a uniform grid of points, at which the Gibbs free energies are calculated for the crystallographic lattices of interest. Then, the sets of alloys are identified naturally on such a grid, which are parallel in composition space to the binary alloys. Such alloys can be designated a name *pseudo*binary alloys, since the composition between their terminal points changes linearly in a multi-component composition space, similarly to the binary alloys. The number of pseudobinary sets in an K-component systems is equal to the combination $C_2^K = \frac{K!}{2!(K-2)!}$. Schematic examples of sets of pseudobinary alloys in ternary and quaternary systems is shown in Fig. 7 and Fig. 8, respectively. For every pseudobinary, a common tangent can be constructed and the phase composition calculated at every grid point. This procedure, however, will yield not one value but a number of values equal to the number of binary alloys in the system. The average phase composition then serves as an approximation for the actual value.

An error arising from averaging can be easily calculated as a standard deviation from the mean, which is helpful in identifying potentially interesting compositions for further research. An upside of such an approach is that the error in the estimation of phase composition is equal to zero for single-phase compositions, which is of interest in the view of identifying single-phase disordered solid solutions.

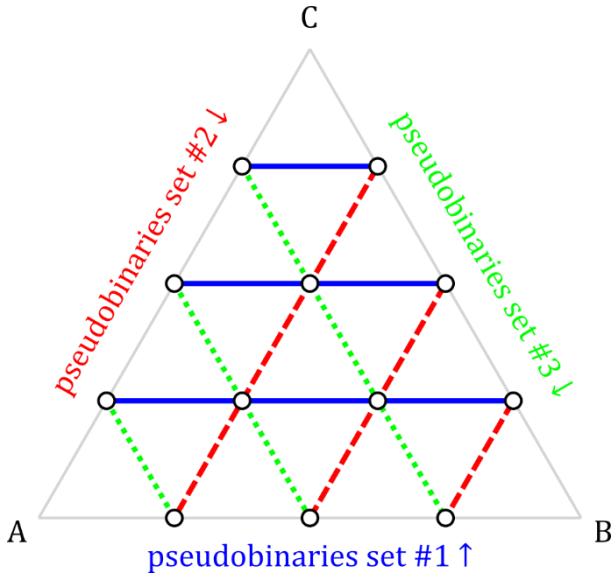

Fig. 7 Uniform grid and pseudobinary sets in the ternary system. Lines with different styles and colors indicate different sets of pseudobinaries.

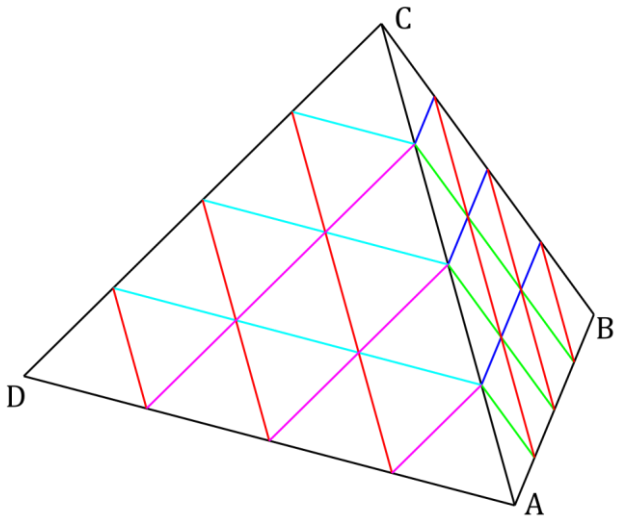

Fig. 8 Pseudobinary sets in quaternary system, shown in different colors. Pseudobinary set parallel to BD binary is not shown due to perspective.

4 Results

This work is in main part based on 2 following publications and their supplementary materials:

1. M. Fedorov, J. S. Wróbel, A. Fernández-Caballero, K. J. Kurzydłowski, D. Nguyen-Manh, Phase stability and magnetic properties in fcc Fe-Cr-Mn-Ni alloys from first-principles modeling, Physical Review B, 101 (2020) 174416 (30), DOI: 10.1103/PhysRevB.101.174416
2. M. Fedorov, J. S. Wróbel, W. Chromiński, G. Cieślak, M. Płocińska, K. J. Kurzydłowski, D. Nguyen-Manh, Composition stability of single fcc phase in Cr-Fe-Mn-Ni alloys: first-principles prediction and experimental validation, Acta Materialia (under review), DOI: 10.2139/ssrn.4156051

This section contains the discussion of the main results from the publications listed above, as well as the results not published previously.

4.1 Phase stability of fcc alloys

Results of the investigation of phase stability of fcc Fe-Cr-Mn-Ni alloys are published in Ref. [61] and presented in Appendix 1.

A database of 1300 fcc structures have been created, and their enthalpies of formation have been calculated using Density Functional Theory. Since fcc structures can exhibit very different forms of magnetism, many structures with the same the composition and configuration $\boldsymbol{\sigma}$ have been considered in various magnetic ordering including non-magnetic, ferromagnetic and different types of ferri- and antiferromagnetic.

Since only configuration $\boldsymbol{\sigma}$ is taken into account in Cluster Expansion, 835 out of 1300 structures have been chosen that possess the most stable magnetic ordering for the same $\boldsymbol{\sigma}$. Magnetic ordering as a function of composition is consistent with available experimental data, see Fig. 8(c) from Appendix 1. The analysis of magnetic properties of Fe-Cr-Mn-Ni structures obtained using DFT enabled to construct the magnetic phase diagram of Fe-Cr-Mn-Ni system.

As described in Section 3.3, the Effective Cluster Interactions in Eq. 3.13 can be derived based on DFT calculations for the considered structures. The number of ECIs was chosen in such a way that the cross-validation error (see Eq. 18 in Appendix 1) between the enthalpies of formation obtained from CE and DFT was the lowest one. In the final version of CE Hamiltonian, the interaction describing the 2-body clusters up to the 6^{th} nearest neighbor, 3-body clusters with maximum distance of 2^{nd} nearest neighbor and one 4-body cluster were

taken into account, which are presented in Fig. 9. For such a set of clusters, the CE Hamiltonian is the following:

$$H_{mix}(\vec{\sigma}) = \sum_{\omega,n} m_{\omega,n} J_{\omega,n} \langle \Gamma_{\omega',n'}(\boldsymbol{\sigma}) \rangle =$$

$$= J_{1,1}^{(0)} \left\langle \Gamma_{1,1}^{(0)} \right\rangle + \sum_{s} J_{1,1}^{(s)} \left\langle \Gamma_{1,1}^{(s)} \right\rangle + \sum_{\mathrm{n}=1}^{6} \sum_{s} m_{2,\mathrm{n}}^{(s)} J_{2,\mathrm{n}}^{(s)} \left\langle \Gamma_{2,\mathrm{n}}^{(s)} \right\rangle \qquad 4.1$$

$$+ \sum_{n=1}^{2} \sum_{s} m_{3,\mathrm{n}}^{(s)} J_{3,\mathrm{n}}^{(s)} \left\langle \Gamma_{3,\mathrm{n}}^{(s)} \right\rangle + \sum_{s} m_{4,1}^{(s)} J_{4,1}^{(s)} \left\langle \Gamma_{4,\mathrm{n}}^{(s)} \right\rangle.$$

The values of ECIs are presented in Table I of Appendix 1.

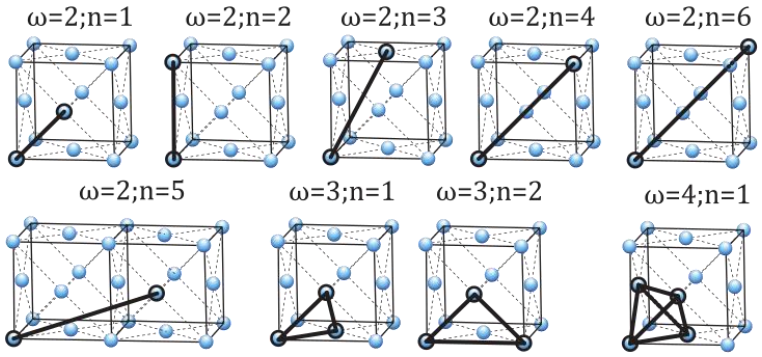

Fig. 9 Considered clusters in fcc Fe-Cr-Mn-Ni system.

Configurational entropy has been included using Eq. 3.22 only for the first nearest neighbor.

The CE model enabled to reproduce the known binary and ternary fcc ground states (see Table II in Appendix 1) and to find the quaternary ground state of fcc Fe-Cr-Mn-Ni system, with no previous mentions in the literature. The composition of this ground state is $FeCr_2MnNi_4$, and its structure is based on the ternary ABC_6-type structure with *I4/mmm* symmetry. See Fig. 10 for atomic and magnetic arrangement of this structure.

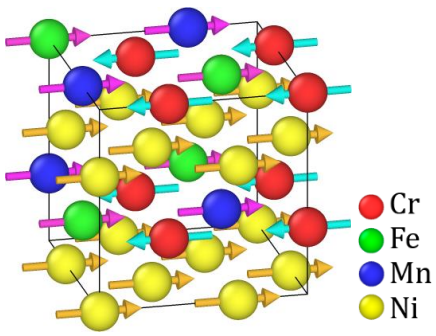

Fig. 10 Quaternary ground state $FeCr_2MnNi_4$ in a conventional fcc unit cell. Magnetic moments are shown with arrows.

Since one of the aims of this work was to identify the concentrations of Fe-Cr-Mn-Ni alloys, for which the disordered alloys (which means the high-entropy alloys) may exist in the widest range of temperatures, the CE model for fcc Cr-Fe-Mn-Ni alloys have been applied in canonical exchange MC simulations in order to study the order-disorder transition temperature, T_{ODT}. The effect of each element on the order-disorder transition temperature has been analyzed using 1-3 pseudobinaries, i.e., pseudobinary alloys where one termination point is a pure element, and the other is a 3-component equiatomic $A_x[BCD]_{100-x}$. Dependency of T_{ODT} on the concentration of each element is shown in Fig. 11.

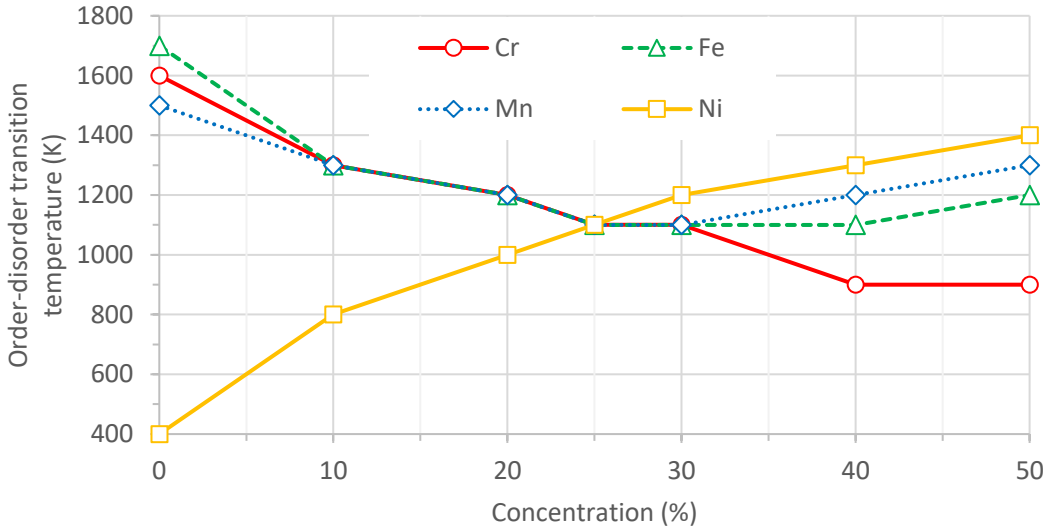

Fig. 11 Order-disorder transition temperature of fcc alloys as a function of concentration of each element. Concentration of the remaining 3 elements is kept equiatomic.

As can be seen in Fig. 11, T_{ODT} for equiatomic Fe-Cr-Mn-Ni is equal to 1100 K. If the equiatomic alloy is depleted of Cr, Fe or Mn, its T_{ODT} increases, meaning that the disordered alloy will be stable only at high temperatures. However, if it is depleted of Ni, a disordered alloy is stable at lower temperatures. This introduces an issue of tradeoff in the properties, since Ni also stabilizes fcc phase.

The order-disorder transition temperatures for the whole range of concentrations of Fe-Cr-Mn-Ni alloys with a concentration mesh equal to 10 at. % are shown in Fig. 16 in Appendix 1. It is observed that the highest T_{ODT} are possessed by the alloys with high concentration of Mn and Ni, which is strongly correlated with the presence of ordered $L1_0$ MnNi phase in the alloys.

4.2 Phase stability of bcc alloys

In order to develop the CE model for bcc Fe-Cr-Mn-Ni alloys, a database of 1062 bcc structures have been created, and their enthalpies of formation have been calculated using Density Functional Theory.

In the final version of CE Hamiltonian, the interactions describing the 2-body clusters up to the 8th nearest neighbor coordination shell, one 3-body cluster and one 4-body cluster were taken into account, which are presented in Fig. 12. For such a set of clusters, the CE Hamiltonian (see Eq. 3.13) is the following:

$$H_{mix}(\vec{\sigma}) = \sum_{\omega,n} m_{\omega,n} J_{\omega,n} \langle \Gamma_{\omega',n'}(\boldsymbol{\sigma}) \rangle =$$

$$= J_{1,1}^{(0)} \left\langle \Gamma_{1,1}^{(0)} \right\rangle + \sum_{s} J_{1,1}^{(s)} \left\langle \Gamma_{1,1}^{(s)} \right\rangle + \sum_{\mathrm{n}=1}^{8} \sum_{s} m_{2,\mathrm{n}}^{(s)} J_{2,\mathrm{n}}^{(s)} \left\langle \Gamma_{2,\mathrm{n}}^{(s)} \right\rangle \qquad 4.2$$

$$+ \sum_{s} m_{3,\mathrm{n}}^{(s)} J_{3,\mathrm{n}}^{(s)} \left\langle \Gamma_{3,\mathrm{n}}^{(s)} \right\rangle + \sum_{s} m_{4,1}^{(s)} J_{4,1}^{(s)} \left\langle \Gamma_{4,\mathrm{n}}^{(s)} \right\rangle.$$

ECIs are presented in Table S1 of Supplementary Material of Appendix 2.

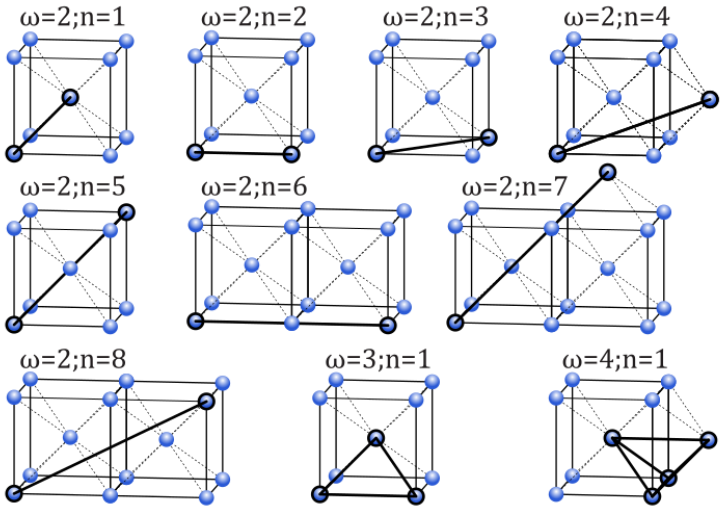

Fig. 12 Considered clusters in bcc Fe-Cr-Mn-Ni system.

Configurational entropy has been calculated using Eq. 3.22 considered only for the first nearest neighbor, since calculation including contribution from farther neighbors produced negative values of formation enthalpy at high temperatures.

Order-disorder transition temperatures for bcc 1-3 pseudobinary alloys ($A_x[BCD]_{100-x}$) are presented in Fig. 13. As can be seen from this figure, T_{ODT} for the equiatomic quaternary alloy is 1000 K. The depletion of equiatomic alloy off Cr, Fe and Mn has a similar effect as in fcc alloys – it increases T_{ODT}. Depleting Ni from 25 at. % to 10 at. %

does not have an effect on T_{ODT}, but if its content reaches below 10 at. %, T_{ODT} also decreases, similarly to fcc alloys.

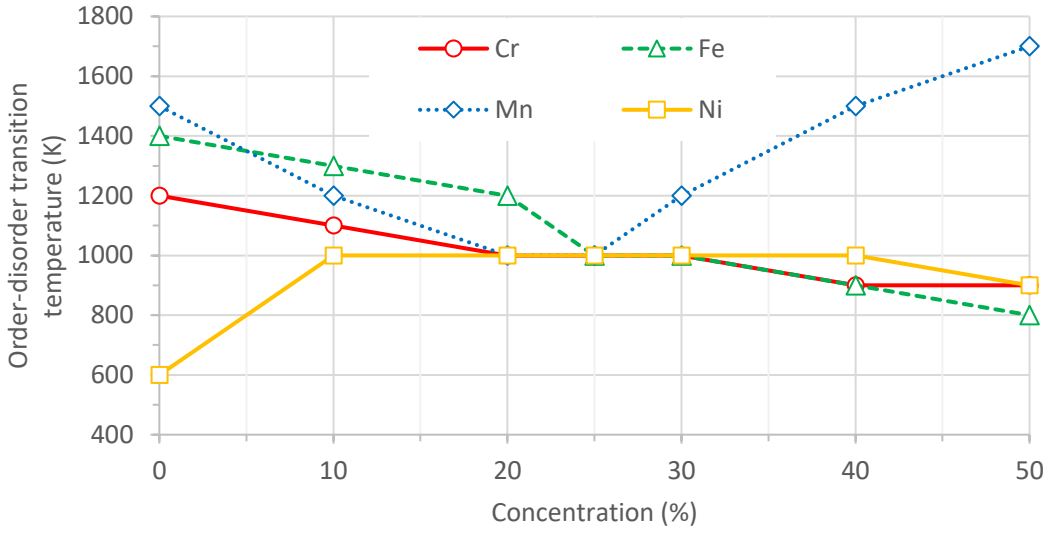

Fig. 13 Order-disorder transition temperature of bcc alloys as a function of concentration of each element. Concentration of the remaining 3 elements is kept equiatomic.

4.3 Relative phase stability of fcc and bcc phases

Detailed analysis of results of investigation of relative phase stability of fcc and bcc phases is presented in Appendix 2. Below are the main results, as well as the ones not presented in the published work.

The analysis of formation enthalpies obtained using DFT calculations for binary fcc and bcc structures in the Fe-Cr-Mn-Ni system enable to indicate the ground state phases and to construct the convex hulls for fcc and bcc systems at 0 K, see Fig. 14. As can be seen in the figure, Ni forms intermetallic fcc phases with negative formation enthalpy with every element present in the system. Equiatomic MnNi has the most negative formation enthalpy not only considering binaries, but in the whole quaternary system, with $H_{form} = -0.157$ eV.

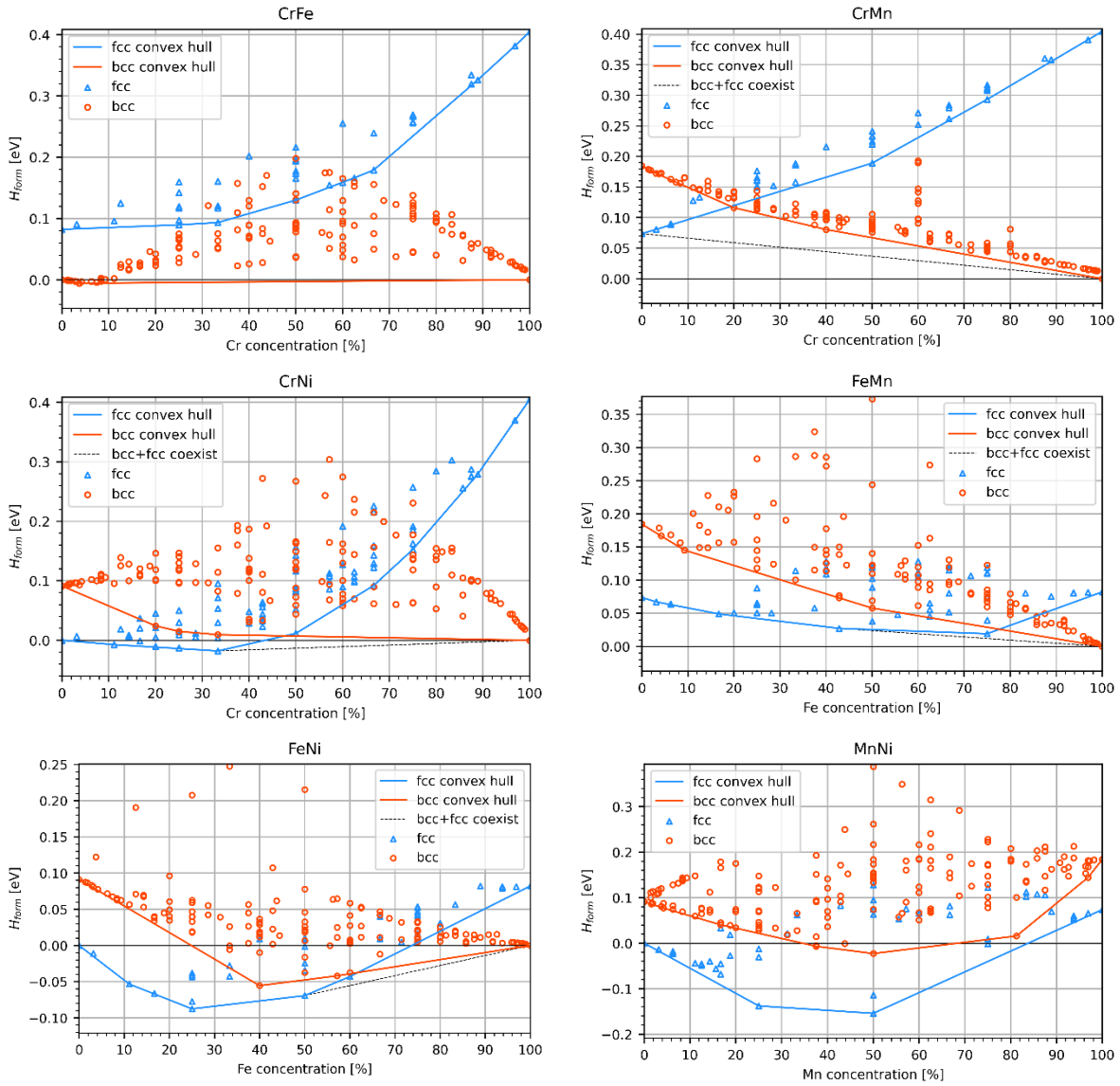

Fig. 14 Convex hulls for fcc and bcc binary alloys in Fe-Cr-Mn-Ni system.

Monte Carlo simulated annealings have been performed on a grid of 5 at. % with 100 K temperature step, resulting in 1767 simulations for each lattice. Common tangent construction and pseudobinary approach have been applied to binary, ternary and quaternary alloys in a sequence described below.

Example of common tangent construction and lever rule calculations of phase composition in binary alloys at 0 K, which was the basis for the subsequent multi-component approach, is presented in Fig. 15.

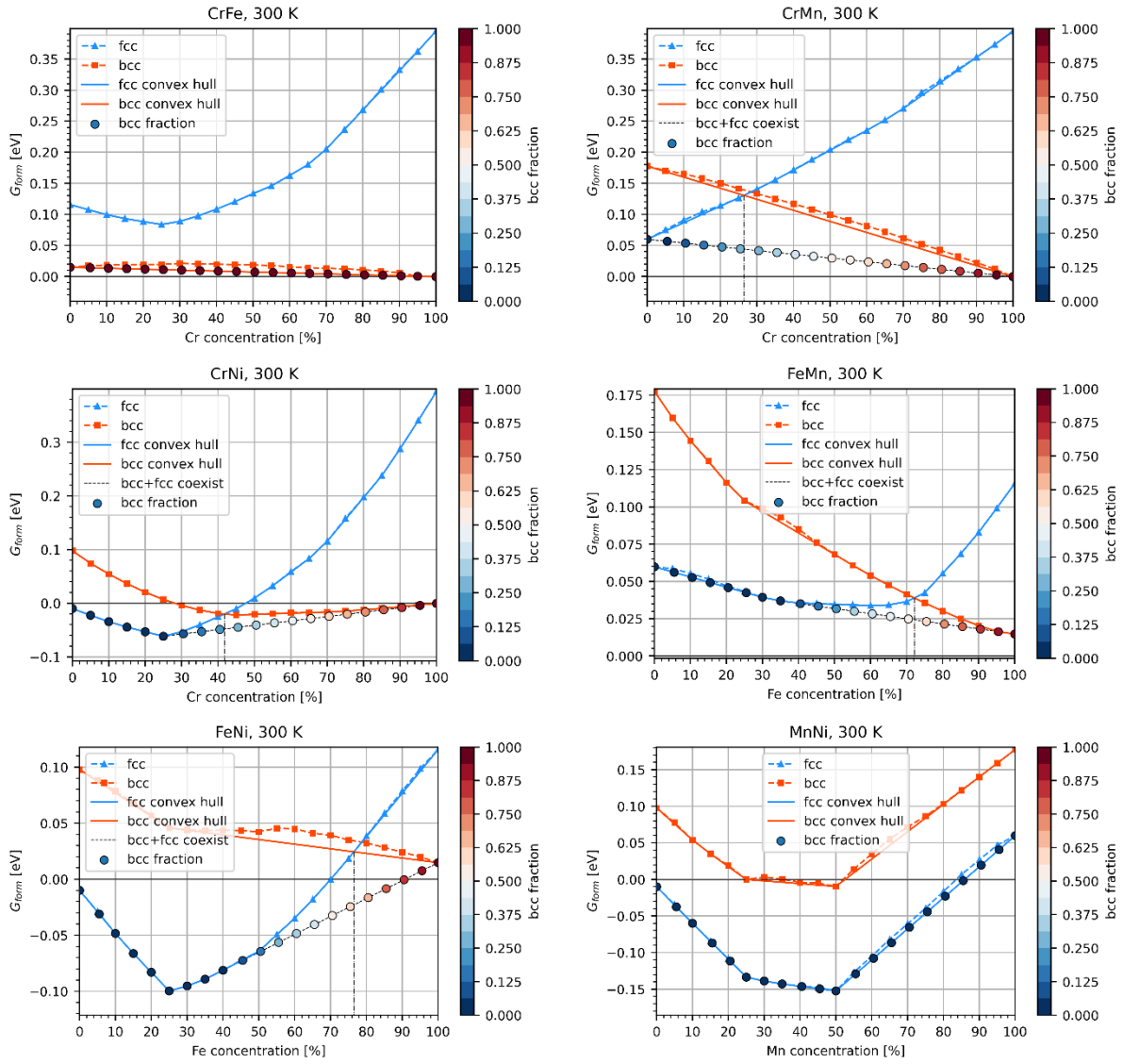

Fig. 15 Common tangent construction for binary alloys at finite temperatures.

In this figure, convex hull is split into 5 at. % segments, for which the phase composition is calculated and indicated by the color gradient, as well as intersection points of fcc and bcc Gibbs free energy curves.

Intersection points do not indicate the point of equal fraction of the two considered phases, but nonetheless they are inherent property of the two shapes, representing Gibbs free energy. For two-component systems, the intersection is the point and as such is found exactly using this classic method. For three-component systems, the energy is represented by surfaces, whose intersection is generally a curve, and as such, the points of intersection of 2-2 pseudobinaries should approximate the said curve. As can be seen in Fig. 16, the points do form a curve, which reassured me to extend this method to four-component system.

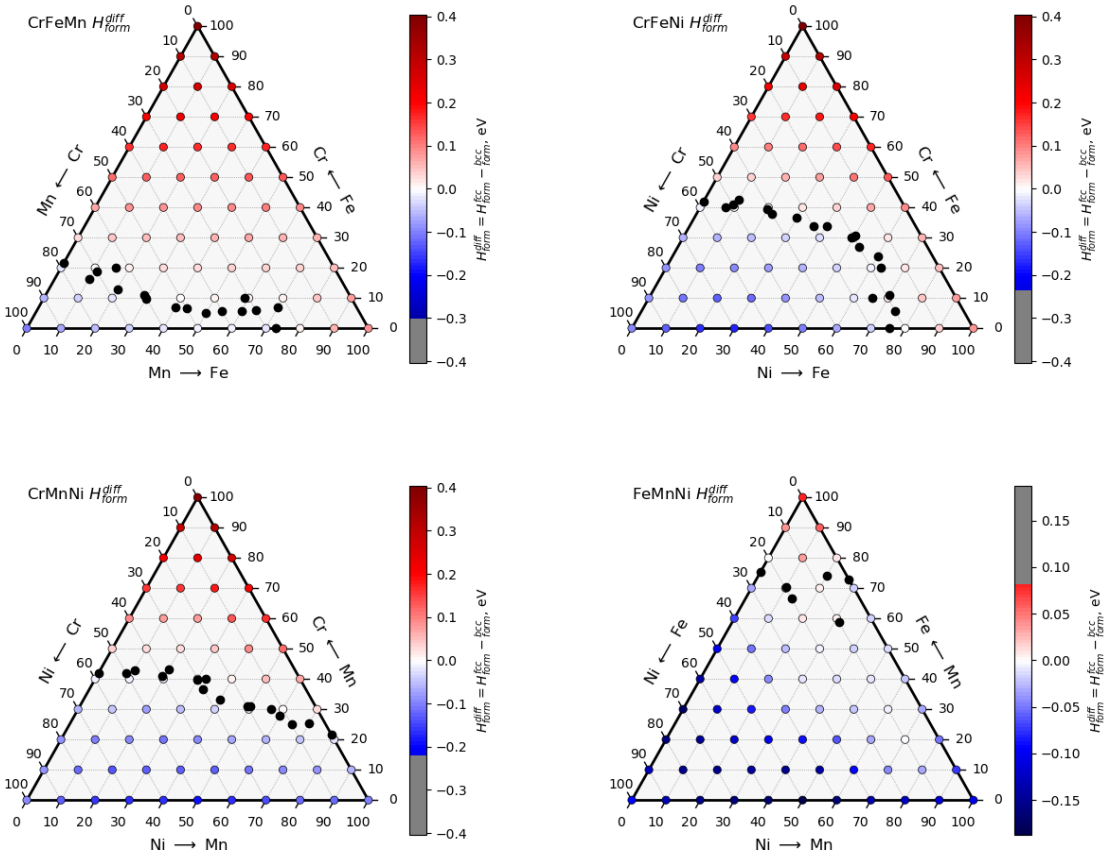

Fig. 16 Intersections of formation enthalpies in ternary alloys.

In a four-component system, the Gibbs free energy is represented by four-dimensional hypersurfaces, for which the intersection is a three-dimensional surface. While exact calculations are complicated, applying the method of 2-2 and 3-3 pseudobinaries intersections produces the intersection points that approximate the surface quite well (see Fig. 17).

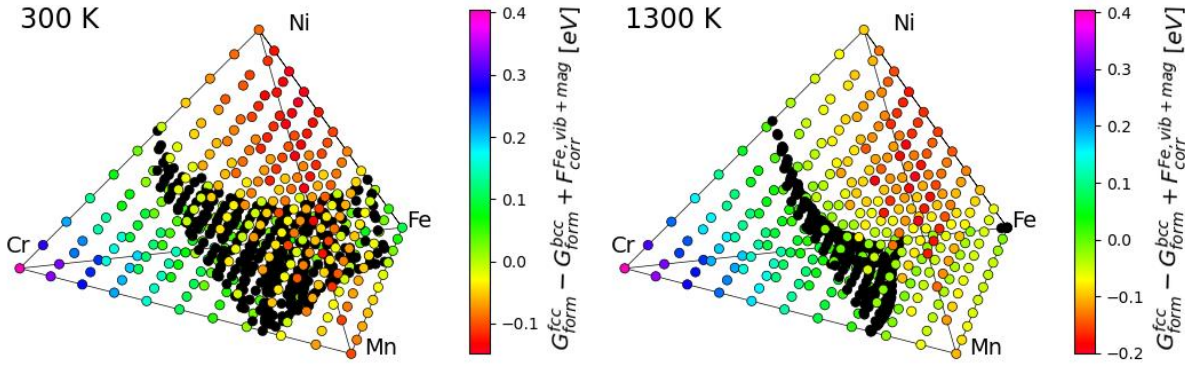

Fig. 17 Gibbs free energy difference of bcc and fcc alloys, shown in color, and a surface of intersections, shown as black points, calculated from 2-2 and 3-3 pseudobinaries. Free energy difference is shown on a sparse grid for better visibility of the intersection points.

With such reassurance that the method of averaging over pseudobinaries can reproduce the features of the multi-dimensional surfaces, it has been applied to calculate the phase composition in the whole range of concentrations in the Fe-Cr-Mn-Ni system. Fig. 18 shows the percentage of fcc phase for alloys in the whole composition range, while the percentage of bcc phase is the remaining value. When compared to Fig. 17, it is visible that the intersection surface indeed splits the phase diagram into predominantly stable fcc and predominantly stable fcc regions, but it lacks details compared to the application of lever rule calculations using the pseudobinary approach.

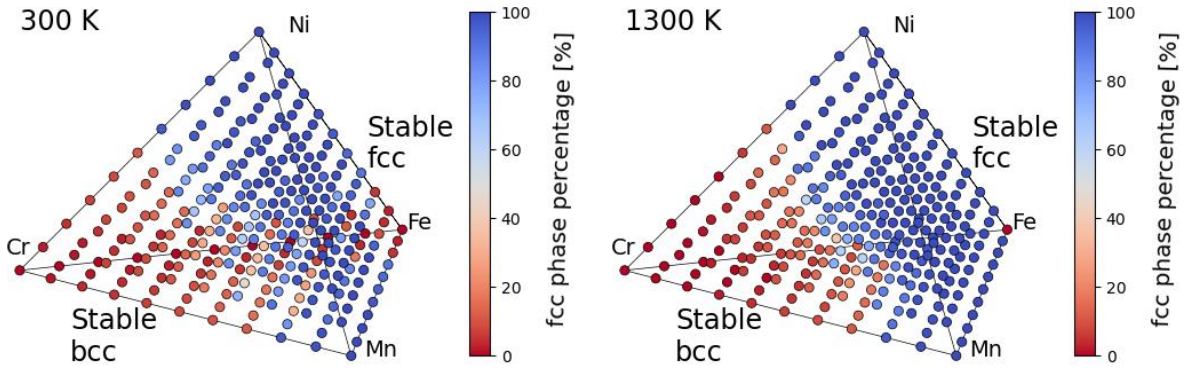

Fig. 18 Phase composition in the whole composition range of Fe-Cr-Mn-Ni alloys, shown on a sparse grid for better visibility of the full diagram.

Fig. 18 should give one a qualitative understanding of the trends in fcc-bcc phase composition in Fe-Cr-Mn-Ni, however, for more a practical understanding, a quantitative analysis can be performed for the effect of each element on phase composition using 1-3 pseudobinaries, similarly to how it has been done for T_{ODT} in Fig. 11 and Fig. 13.

Fig. 19 presents the heatmap of fcc percentage in terms of concentration-temperature coordinates for 4 pseudobinaries, corresponding to each element. In order to present a uniform diagram, the points off-grid are interpolated with inverse distance weighting. This figure is best viewed along with Fig. 20, which shows the standard error of the mean for the same composition-temperature coordinates.

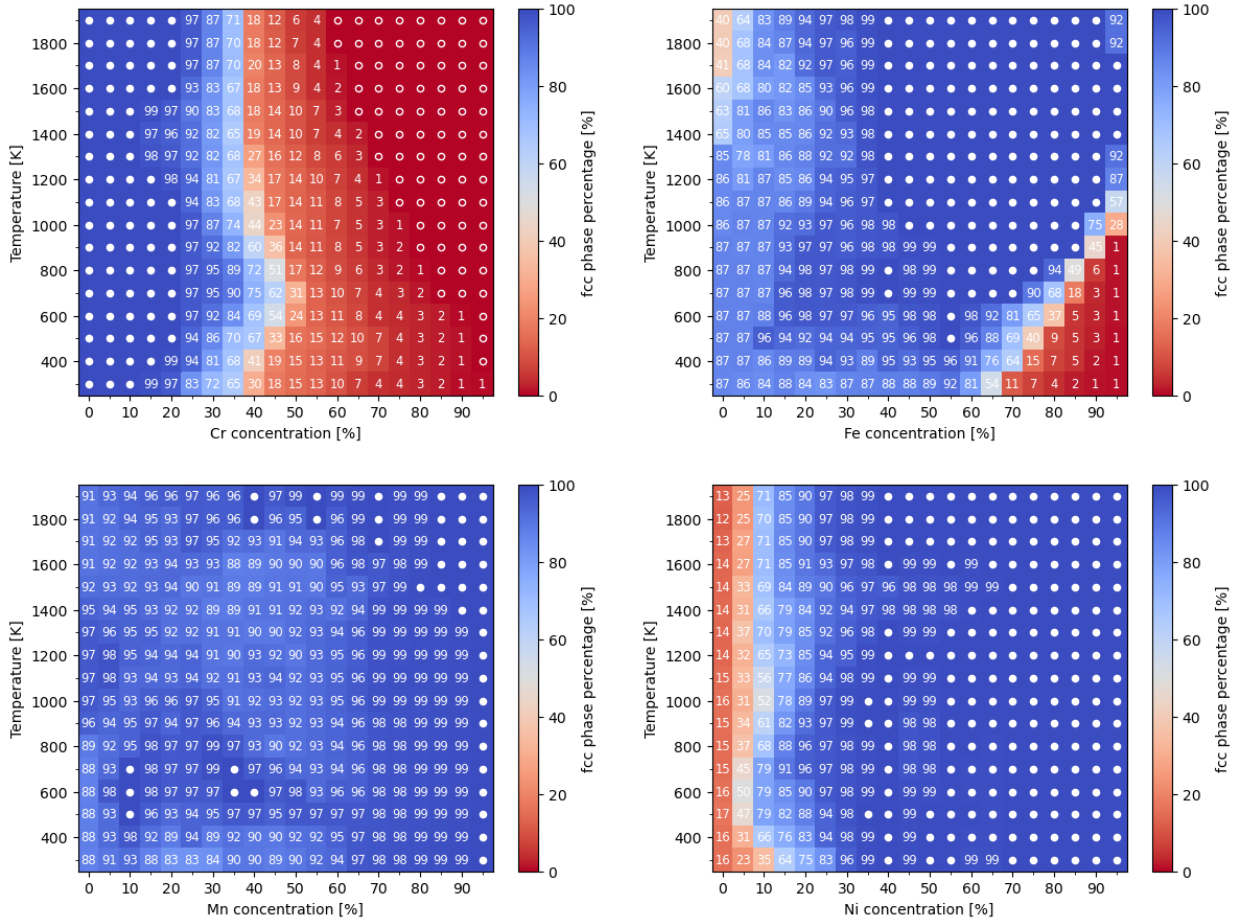

Fig. 19 Composition-temperature heatmaps showing fcc fraction in the Cr-Fe-Mn-Ni alloys according to the common tangent as a function of temperature and concentration of Cr, Fe, Mn and Ni. In order to improve the readability of the figure, 100% fcc is marked with filled circles (●), and 0% fcc is marked with open circles (○). Data for compositions off-grid is interpolated with inverse distance weighting.

The first most noticeable effect when comparing Fig. 19 and Fig. 20 is that the errors for points where only one phase is predicted to be stable are equal to zero, while the highest errors are observed in the regions of coexistence of fcc and bcc phases. This adds a good quantitative measure factor for deciding which alloys might be chosen for experimental studies.

For alloys with Cr content up to 10 at. % Cr, the single fcc phase is stable at all temperatures. For Cr concentrations of 15 and 20 at. %, the bcc fraction is not larger than 4 %, indicating with 95 % confidence that the single fcc phase is stable for those compositions. In contrast, a single bcc phase can be observed for all Cr concentrations larger than 50 at. % Cr. However, the errors increase with decreasing temperature and Cr concentration, suggesting that a small fraction of the fcc phase might be observed for alloys with lower Cr content and lower temperature. For the pseudobinary alloys with Cr concentration between 30 and 50 at.% Cr, both fcc and bcc phases are found to coexist. An important composition is the four-component

equiatomic, for which the fraction of fcc phase is decreased down to 90 % at 1500 K. The error for that temperature is equal to 17 %, which means that with 95 % confidence, the fcc phase can still be observed, however, the coexistence of the two phases is possible.

The stability of the fcc phase in Fe-rich alloys is temperature-dependent, with the bcc fraction dominating at low temperatures. For instance, below 1000 K for the pseudobinary alloy with 95 at. % Fe. At higher temperatures, the fcc phase becomes more stable. The fcc-bcc phase transition temperature decreases with decreasing Fe content, and for the alloy with 55 at. % Fe, a single fcc phase is formed above 500 K.

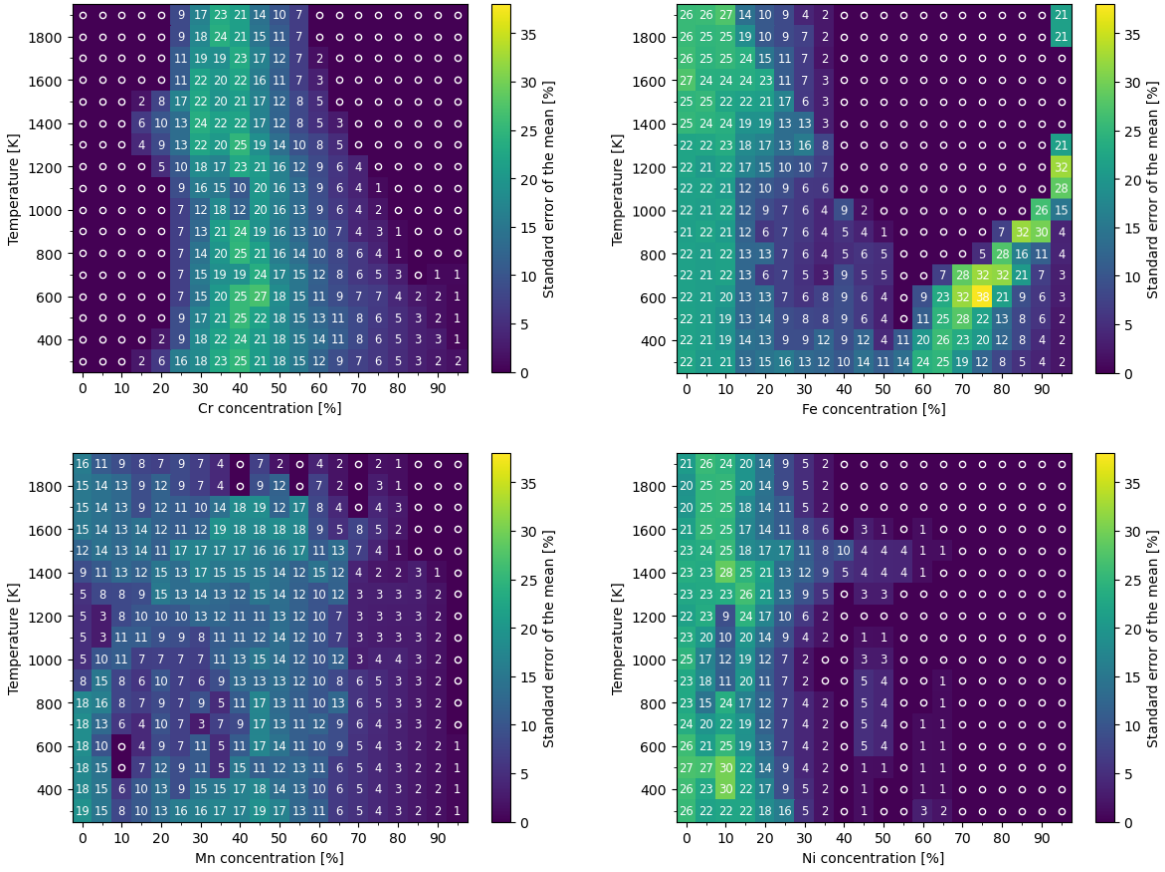

Fig. 20 Error in composition heat-maps showing standard derivations from the mean fcc fraction for the Cr-Fe-Mn-Ni alloys as a function of temperature and concentration of Cr, Fe, Mn and Ni, coming from the averaging of the results over six pseuudobinary sets. Errors for compositions off-grid are interpolated with inverse distance weighting.

The fcc phase is dominant in Mn pseudobinary alloys for all considered Mn concentrations and temperatures. This observation is potentially important for the design of Cr-Fe-Mn-Ni-based high-entropy alloys, given the significantly higher Mn concentration in these materials than in austenitic steels. With 95% confidence, the single fcc phase can be observed for most Mn alloys, while the bcc fraction is usually smaller than the corresponding errors. This

observation coincides with the empirical correlation of valent electron concentration with the stability of HEAs with different crystallographic lattices. For VEC<6.67, the bcc lattice should be more stable, while for VEC>8, bcc lattice is stable. Since VEC of Mn is 7, it lies in the region of coexistence of two phases, thus not providing any preference. It should be noted that the alpha-Mn phase is not considered in this work, and the phase of structures in the Mn-rich region is likely to be alpha-Mn solid solution rather than fcc.

For Ni pseudobinary alloys, fcc phase is with 95 % confidence stable for the alloys with Ni content higher than 25 at. %. If the bcc fraction is observed, its percentage is not larger than 6 % and is usually below the errors provided for corresponding compositions and temperatures. In contrary to Ni-rich alloys, the Cr-Fe-Mn-Ni alloys with a low Ni concentration consist mainly of the bcc phase.

By analyzing the fractions of the fcc phase for whole considered alloy concentrations, I was able to identify the alloy compositions for which the single fcc phase is stable for a wide range of temperatures. In Fig. 21, there are shown the predicted phase compositions for the best near-equiatomic alloys, for which the fcc percentage is equal to 100 % for a wide range of temperatures. The order-disorder transition temperatures are also given in the legend of the figures. Among the considered near-equiatomic alloys, $Cr_{20}Fe_{35}Mn_{20}Ni_{25}$ and $Cr_{15}Fe_{30}Mn_{25}Ni_{30}$ are indicated as those with good stability of fcc phase and low order-disorder transition temperature.

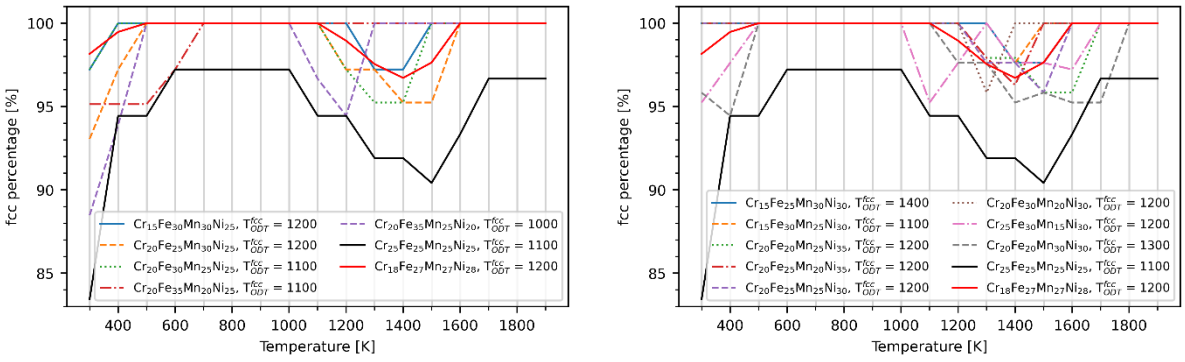

Fig. 21 Percentage of fcc in the near-equiatomic Cr-Fe-Mn-Ni alloys with 20 and 25 at. % Ni and 30 and 35 at. % Ni. All presented compositions have deviations from 100% fcc that are smaller than the precision error of calculating the phase percentage. The equiatomic composition (black solid line) and the ORNL composition from Ref. [10], Cr18Fe27Mn27Ni28, (red solid line) are also plotted for reference. In the legend, there is also provided information about order-disorder transition temperature for the considered fcc alloys (in K).

4.4 Magnetic properties of fcc and bcc alloys

Analysis of magnetic properties of both fcc and bcc alloys has been performed for the structures calculated during the construction of the databases for Cluster Expansion model construction. Apart from magnetic phase diagram, shown in Fig. 11 of Appendix 1, a correlation can be found between the average magnitude of magnetic moment (AMMM) and the volume of the structure normalized per atom. Such correlation shows how much does magnetic system responds to the changes in volume, introduced by e.g., mechanical stress or irradiation effects.

In view of the current work, it is interesting to find the difference between the magneto-volume properties of Fe-Cr-Ni and Fe-Cr-Mn-Ni, since the latter has improved magnetic properties compared to the former. This analysis is presented in Fig. 22.

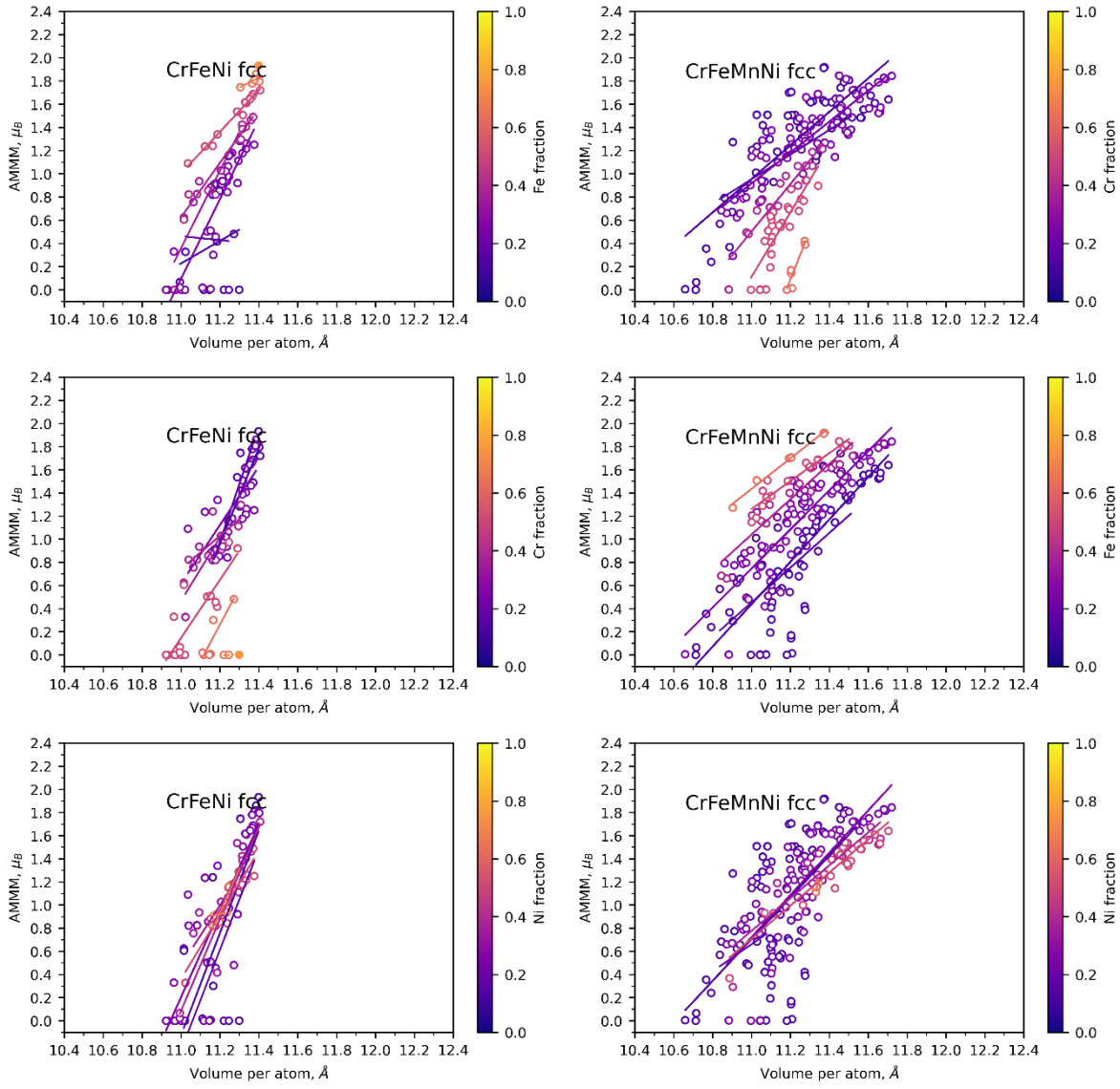

Fig. 22 Magneto-volume relation for fcc Fe-Cr-Ni (left column) and Fe-Cr-Mn-Ni (right column).

As can be seen in Fig. 22, adding Mn does not affect the range of magnetic moments – the maximum average magnitude of magnetic moments observed in the system is $2\,\mu_B$. However, the volume per atom is much more spread for Fe-Cr-Mn-Ni structures compared to Fe-Cr-Ni structures. This can be interpreted in the following way. Since neutron irradiation introduces non-equilibrium vacancies that increase the volume per atom, the increased magnetic moments correlated with the vacancies may hinder the diffusion of self-interstitial atoms. If the system does not have such a strong increase in AMMM, the diffusion of self-interstitial atoms should not be slowed, and the self-interstitial atoms can recombine with vacancies faster, thus not promoting the growth of the voids. This hypothesis should be tested in the consequent research.

5 Summary

Aiming at finding of alloys, potentially important for the nuclear applications, a sizeable theoretical model has been created with a fully theoretical approach. Each step of the model allowed for various insights and observation, which helped to achieve a set goal. A detailed description of the findings is presented in the two published works, and the main findings are as follows:

1. A large database of structures with fcc and bcc crystallographic lattices in the whole composition range of Fe-Cr-Mn-Ni system has been created. Its validity is supported by the correctly predicted ground states from literature. A new stable quaternary ground state has been found.
2. Calculation of the various magnetic configurations in the fcc Fe-Cr-Mn-Ni system and the subsequent analysis of their stability produced a quaternary magnetic phase diagram at 0 K. Diagram reproduces the magnetic properties of binary and ternary alloys found in literature, which provides additional support for the model.
3. The exchange MC simulations using the DFT-based CE models for fcc and bcc Fe-Cr-Mn-Ni systems enables to study the phase stability of Fe-Cr-Mn-Ni alloys. The analysis of order-disorder transition enables to identify the alloy compositions for which the disordered alloys are stable for the wide range of temperatures, where the alloys can be treated as disordered high-entropy alloys.
4. The effect of each element on the relative phase stability of fcc and bcc alloys is of fcc and bcc alloys is investigated by an application of the common tangent construction procedure and averaging over the results for pseudobinary alloys.
5. Cr significantly stabilizes bcc lattice, and its presence is undesirable in concentrations higher than 20 at. %. Pure Fe undergoes phase transformation at 1000 K, above which it has fcc lattice, and below – bcc lattice. However, 100% fcc phase can be observed at low temperature in alloys with Fe concentration as high as 50 at. %.
6. Ni, having fcc lattice in the whole range of temperatures, stabilizes the fcc phase, which is desirable. However, Ni forms ordered structures with negative formation enthalpy with all other elements present in the system. This can result in the formation of intermetallic phases, which are known to be undesirably brittle, during the production and application of the alloys.
7. Mn as a member of the four-component system, does not seem to have a preference in stabilizing either fcc or bcc lattice. While seemingly unremarkable, it means that

Mn can be used as a filler component, at the same time adding compositional complexity and improving irradiation-resistant properties. Additionally, Mn introduces wider variability of volume in view of magneto-volume relation when comparing the Fe-Cr-Mn-Ni system to the Fe-Cr-Ni system. This provides an additional potential explanation of increased irradiation properties since in quaternary alloys the changes of volume induced by irradiation defects produce less magnetic frustration, which in turn hinders diffusion and annihilation of defects to a lower amount compared to Fe-Cr-Ni.

8. Mn and Ni have a synergetic effect, forming the most stable intermetallic structure in the whole composition range of Fe-Cr-Mn-Ni system – antiferromagnetic $L1_0$-MnNi. It is stable up to the melting point and, indeed, has been observed to form in different multi-principal element alloys containing Mn and Ni. The way to reduce the formation of said intermetallic is to keep the concentration of Mn and Ni inequal.
9. Methodology developed for the analysis of phase stability of multi-component systems is simple, straightforward, and does not require additional approximations. While it has errors, they can be calculated exactly, and they are not present in or near the single-phase regions. Results of the application of said methodology coincide with the experimental results reported in the literature, as well as the ones performed at the Faculty of Materials Science and Engineering (FMSE), with a good qualitative and satisfactory quantitative agreement.
10. Applying this methodology, the near-equiatomic alloy compositions as $Cr_{20}Fe_{35}Mn_{20}Ni_{25}$ and $Cr_{15}Fe_{30}Mn_{25}Ni_{30}$ are indemnified as alloys that can form disordered single phase for a wide range of temperatures. The prediction of single fcc phase for $[CrFeMn]_{65}Ni_{35}$ alloy was validated positively by the experiments performed at FMSE. They have not been reported in the literature yet, and thus, can potentially be of interest for further studies searching for fcc multi-principal element disordered solid solution alloys. These results confirm the hypothesis posed in this work that there exist unidentified multi-principal element alloys in the Fe-Cr-Mn-Ni system possessing stable disordered single fcc phase that can be found with a purely theoretical approach.

6 References

[1] D.C. Roberts, Climate Change 2022 : Impacts , Adaptation and Vulnerability Working Group II Contribution to the Sixth Assessment Report of the Intergovernmental Panel on Climate Change, 2022.

[2] Main farm indicators by agricultural area, type and economic size of the farm, share of consumed production, legal status of the holding and NUTS2 region [EF_M_FARMLEG], (n.d.). https://ec.europa.eu/eurostat/databrowser/bookmark/1c164b2e-ca9d-4cdd-811b-614f7b21cd3c?lang=en.

[3] United Nations Environment Programme, Emissions Gap Report 2022: The Closing Window — Climate crisis calls for rapid transformation of societies, Nairobi, 2022.

[4] G. Federici, W. Biel, M.R. Gilbert, R. Kemp, N. Taylor, R. Wenninger, European DEMO design strategy and consequences for materials, Nucl. Fusion. 57 (2017) 092002(26).

[5] B.J. Yeh, S. Chen, S. Lin, J. Gan, T. Chin, T. Shun, C. Tsau, Nanostructured High-Entropy Alloys with Multiple Principal Elements : Novel Alloy Design Concepts and Outcomes, Adv. Eng. Mater. 6 (2004) 299–303.

[6] B. Cantor, I.T.H. Chang, P. Knight, A.J.B. Vincent, Microstructural development in equiatomic multicomponent alloys, Mater. Sci. Eng. A. 375–377 (2004) 213–218.

[7] A.S. Sharma, S. Yadav, K. Biswas, B. Basu, High-entropy alloys and metallic nanocomposites: Processing challenges, microstructure development and property enhancement, Mater. Sci. Eng. R. 131 (2018) 1–42.

[8] J.-W. Yeh, Recent progress in high-entropy alloys, Ann. Chim. Sci. Des Matériaux. 31 (2006) 633–648.

[9] D.B. Miracle, O.N. Senkov, A critical review of high entropy alloys and related concepts, Acta Mater. 122 (2017) 448–511.

[10] Y. Shi, B. Yang, P.K. Liaw, Corrosion-resistant high-entropy alloys: A review, Metals (Basel). 7 (2017) 1–18.

[11] A.V. Kuznetsov, D.G. Shaysultanov, N.D. Stepanov, G.A. Salishchev, O.N. Senkov, Tensile properties of an AlCrCuNiFeCo high-entropy alloy in as-cast and wrought conditions, Mater. Sci. Eng. A. 533 (2012) 107–118.

[12] N.D. Stepanov, D.G. Shaysultanov, M.A. Tikhonovsky, G.A. Salishchev, Tensile properties of the Cr-Fe-Ni-Mn non-equiatomic multicomponent alloys with different Cr contents, Mater. Des. 87 (2015) 60–65.

[13] O.N. Senkov, S. V. Senkova, C. Woodward, Effect of aluminum on the microstructure

and properties of two refractory high-entropy alloys, Acta Mater. 68 (2014) 214–228.

[14] F.J. Wang, Y. Zhang, G.L. Chen, Atomic packing efficiency and phase transition in a high entropy alloy, J. Alloys Compd. 478 (2009) 321–324.

[15] O. El-Atwani, N. Li, M. Li, A. Devaraj, J.K.S. Baldwin, M.M. Schneider, D. Sobieraj, J.S. Wróbel, D. Nguyen-Manh, S.A. Maloy, E. Martinez, Outstanding radiation resistance of tungsten-based high-entropy alloys, Sci. Adv. 5 (2019) 1–28.

[16] N.A.P.K. Kumar, C. Li, K.J. Leonard, H. Bei, S.J. Zinkle, Microstructural stability and mechanical behavior of FeNiMnCr high entropy alloy under ion irradiation, Acta Mater. 113 (2016) 230–244.

[17] C. Li, J. Yin, K. Odbadrakh, B.C. Sales, S.J. Zinkle, G.M. Stocks, B.D. Wirth, First principle study of magnetism and vacancy energetics in a near equimolar NiFeMnCr high entropy alloy, J. Appl. Phys. 125 (2019) 155103(17).

[18] K. Jin, C. Lu, L.M. Wang, J. Qu, W.J. Weber, Y. Zhang, H. Bei, Effects of compositional complexity on the ion-irradiation induced swelling and hardening in Ni-containing equiatomic alloys, Scr. Mater. 119 (2016) 65–70.

[19] C. Lu, L. Niu, N. Chen, K. Jin, T. Yang, P. Xiu, Y. Zhang, F. Gao, H. Bei, S. Shi, M.R. He, I.M. Robertson, W.J. Weber, L. Wang, Enhancing radiation tolerance by controlling defect mobility and migration pathways in multicomponent single-phase alloys, Nat. Commun. 7 (2016) 1–8.

[20] R.L. Klueh, D.R. Harries, High-Chromium Ferritic and Martensitic Steels for Nuclear Applications, ASTM International, 2001. https://app.knovel.com/hotlink/toc/id:kpHCFMSNA3/high-chromium-ferritic/high-chromium-ferritic.

[21] T. Toyama, Y. Nozawa, W. Van Renterghem, Y. Matsukawa, M. Hatakeyama, Y. Nagai, Grain boundary segregation in neutron-irradiated 304 stainless steel studied by atom probe tomography, J. Nucl. Mater. 425 (2012) 71–75.

[22] D.H. Chung, W.C. Kim, S.Y. Baek, M.H. Kim, Y.S. Na, Thermodynamics-based design strategy for optimizing strength and ductility of Cr-Ni-Mn-Fe medium-entropy alloys, J. Alloys Compd. 899 (2022).

[23] Z. Wu, H. Bei, F. Otto, G.M. Pharr, E.P. George, Recovery, recrystallization, grain growth and phase stability of a family of FCC-structured multi-component equiatomic solid solution alloys, Intermetallics. 46 (2014) 131–140.

[24] Z. Wu, H. Bei, Microstructures and mechanical properties of compositionally complex Co-free FeNiMnCr18 FCC solid solution alloy, Mater. Sci. Eng. A. 640 (2015) 217–224.

[25] Y. Zhang, H. Wu, X. Yu, D. Tang, R. Yuan, H. Sun, Microstructural evolution and strengthening mechanisms in CrxMnFeNi high-entropy alloy, J. Mater. Res. Technol. 12 (2021) 2114–2127.

[26] J. Zhou, H. Liao, H. Chen, A. Huang, Microstructure and Tensile Mechanical Behavior of a Single-Phase Fe35Mn10Cr20Ni35 High-Entropy Alloy, J. Mater. Eng. Perform. 30 (2021) 3352–3362.

[27] A. Fernández-Caballero, E. Bousser, S.M. Shubeita, P.T. Wady, Y. Gu, R. Krishna, M.J. Gorley, D. Nguyen-Manh, P.M. Mummery, E.J. Pickering, High-dose ion irradiation damage in Fe28Ni28Mn26Cr18 characterised by TEM and depth-sensing nanoindentation, Nucl. Mater. Energy. 28 (2021).

[28] A. Kamboj, E.A. Marquis, Effect of dose rate on the phase stability of a CrFeNiMn alloy, Scr. Mater. 215 (2022) 114697.

[29] J. Lehtonen, Y. Ge, N. Ciftci, O. Heczko, V. Uhlenwinkel, S.P. Hannula, Phase structures of gas atomized equiatomic CrFeNiMn high entropy alloy powder, J. Alloys Compd. 827 (2020) 154142.

[30] J. Lehtonen, P. Lehto, Y. Ge, A. Juselius, S.-P. Hannula, Mechanical properties of pulsed electric current sintered CrFeNiMn equiatomic alloy, Mater. Sci. Eng. A. 842 (2022) 143071.

[31] C. Li, X. Hu, T. Yang, N.K. Kumar, B.D. Wirth, S.J. Zinkle, Neutron irradiation response of a Co-free high entropy alloy, J. Nucl. Mater. 527 (2019) 151838.

[32] T.J. Manescau, J. Braun, O. Dezellus, Computational development, synthesis and mechanical properties of face centered cubic Co-free high entropy alloys, Mater. Today Commun. 30 (2022) 103202.

[33] R.K. Nutor, M. Azeemullah, Q.P. Cao, X.D. Wang, D.X. Zhang, J.Z. Jiang, Microstructure and properties of a Co-free Fe50Mn27Ni10Cr13 high entropy alloy, J. Alloys Compd. 851 (2021) 156842.

[34] N.D. Stepanov, D.G. Shaysultanov, M.A. Tikhonovsky, G.A. Salishchev, Tensile properties of the Cr-Fe-Ni-Mn non-equiatomic multicomponent alloys with different Cr contents, Mater. Des. 87 (2015) 60–65.

[35] Y. Ikeda, B. Grabowski, F. Körmann, Ab initio phase stabilities and mechanical properties of multicomponent alloys: A comprehensive review for high entropy alloys and compositionally complex alloys, Mater. Charact. 147 (2019) 464–511.

[36] M. Born, R. Oppenheimer, Zur Quantentheorie der Molekeln, Ann. Phys. 389 (1927) 457–484.

[37] P. Hohenberg, W. Kohn, Inhomogeneous electron gas, Phys. Rev. 136 (1964) 864–871.

[38] W. Kohn, L.J. Sham, Self-Consistent Equations Including Exchange and Correlation Effects, Phys. Rev. 140 (1965) 1133–1138.

[39] H.J. Monkhorst, J.D. Pack, Special points for Brillouin-zone integrations, Phys. Rev. B. 13 (1976) 5188–5192.

[40] D. Vanderbilt, Soft self-consistent pseudopotentials in a generalized eigenvalue formalism, Phys. Rev. B. 41 (1990) 7892–7895.

[41] P.E. Blöchl, Projector augmented-wave method, Phys. Rev. B. 50 (1994) 17953–17979.

[42] J.P. Perdew, K. Burke, M. Ernzerhof, Generalized gradient approximation made simple, Phys. Rev. Lett. 77 (1996) 3865–3868.

[43] G. Kresse, J. Furthmüller, Efficient iterative schemes for ab initio total-energy calculations using a plane-wave basis set, Phys. Rev. B. 54 (1996) 11169–11186.

[44] G. Kresse, J. Furthmüller, Efficiency of ab-initio total energy calculations for metals and semiconductors using a plane-wave basis set, Comput. Mater. Sci. 6 (1996) 15–50.

[45] G. Kresse, D. Joubert, From ultrasoft pseudopotentials to the projector augmented-wave method, Phys. Rev. B. 59 (1999) 1758–1775.

[46] J.M. Sanchez, F. Ducastelle, D. Gratias, Generalized cluster description of multicomponent systems, Physica A. 128 (1984) 334–350.

[47] A. van de Walle, Multicomponent multisublattice alloys, nonconfigurational entropy and other additions to the Alloy Theoretic Automated Toolkit, Calphad Comput. Coupling Phase Diagrams Thermochem. 33 (2009) 266–278.

[48] J.W.D. Connolly, A.R. Williams, Density-functional theory applied to phase transformations in transition-metal alloys, Phys. Rev. B. 27 (1983) 5169–5172.

[49] A. van de Walle, G. Ceder, Automating first-principles phase diagram calculations, J. Phase Equilibria. 23 (2002) 348–359.

[50] A. van de Walle, M. Asta, G. Ceder, The alloy theoretic automated toolkit: A user guide, Calphad Comput. Coupling Phase Diagrams Thermochem. 26 (2002) 539–553.

[51] A. van de Walle, M. Asta, Self-driven lattice-model Monte Carlo simulations of alloy thermodynamic properties and phase diagrams, Model. Simul. Mater. Sci. Eng. 10 (2002) 521–538.

[52] Y. Zhang, S. Guo, C.T. Liu, X. Yang, High-Entropy Alloys, Springer, Cham, 2016.

[53] F. Körmann, Y. Ikeda, B. Grabowski, M.H.F. Sluiter, Phonon broadening in high entropy alloys, Npj Comput. Mater. 3 (2017) 36(9).

[54] D. Ma, B. Grabowski, F. Körmann, J. Neugebauer, D. Raabe, Ab initio thermodynamics

of the CoCrFeMnNi high entropy alloy: Importance of entropy contributions beyond the configurational one, Acta Mater. 100 (2015) 90–97.

[55] I. Toda-Caraballo, J.S. Wróbel, D. Nguyen-Manh, P. Pérez, P.E.J. Rivera-Diaz-del-Castillo, Simulation and Modeling in High Entropy Alloys, JOM. 69 (2017) 2137–2149.

[56] A. Van de Walle, G. Ceder, The effect of lattice vibrations on substitutional alloy thermodynamics, Rev. Mod. Phys. 74 (2002) 11–45.

[57] W.L. Bragg, E.J. Williams, The effect of thermal agitation on atomic arrangement in alloys, Proc. R. Soc. A. 145 (1934) 699–730.

[58] H.A. Bethe, Statistical Theory of Superlattices, 145 (1935) 245–270.

[59] E.A. Guggenheim, Statistical thermodynamics of mixtures with non-zero energies of mixing, Proc. R. Soc. London. Ser. A. Math. Phys. Sci. 183 (1944) 213–227.

[60] A. Fernandez-Caballero, M. Fedorov, J.S. Wróbel, P.M. Mummery, D. Nguyen-manh, Configurational Entropy in Multicomponent Alloys: Matrix Formulation from Ab Initio Based Hamiltonian and Application to the FCC Cr-Fe-Mn-Ni System, Entropy. 21 (2019) 68(19).

[61] M. Fedorov, J.S. Wróbel, A. Fernández-Caballero, K.J. Kurzydłowski, D. Nguyen-Manh, Phase stability and magnetic properties in fcc Fe-Cr-Mn-Ni alloys from first-principles modeling, Phys. Rev. B. 101 (2020) 174416(30).